

Fusion and Direct Reactions of Halo Nuclei at Energies around the Coulomb Barrier

N. Keeley¹, R. Raabe², N. Alamanos¹, J. L. Sida³

¹CEA DSM/DAPNIA/SPhN, F-91191 Gif-sur-Yvette, France

²Instituut voor Kern- en Stralingsfysica, K.U.Leuven,
Celestijnenlaan 200 D, B-3001 Leuven, Belgium

³CEA DIF/DPTA/Service de Physique Nucléaire,
F-91680 Bruyères-le-Châtel, France

October 2, 2018

Abstract

The present understanding of reaction processes involving light unstable nuclei at energies around the Coulomb barrier is reviewed. The effect of coupling to direct reaction channels on elastic scattering and fusion is investigated, with the focus on halo nuclei, for which such effects are expected to be most important. With the aim of resolving possible ambiguities in the terminology a short list of definitions for the relevant processes and quantities is proposed. This is followed by a review of the experimental and theoretical tools and information presently available. The effect of breakup couplings on elastic scattering and of transfer couplings on fusion is investigated with a series of model calculations within the coupled-channels framework. The experimental data on fusion are then compared to “bare” no-coupling one-dimensional barrier penetration model calculations employing reasonably realistic double-folded potentials. On the basis of these model calculations and comparisons with experimental data, conclusions are drawn from the observation of recurring features. The total fusion cross sections for halo nuclei show a suppression with respect to the “bare” calculations at energies just above the barrier that is probably due to single neutron transfer reactions. The data for total fusion are also consistent with a possible sub-barrier enhancement; however, this observation is not conclusive and other couplings besides the single-neutron channels would be needed in order to explain any actual enhancement. We find that a characteristic feature of halo nuclei is the dominance of direct reactions over fusion at near and sub-barrier energies; the main part of the cross section is related to neutron transfers, while calculations indicate only a modest contribution from the breakup process.

Contents

1	Introduction	2
2	Definitions	4
2.1	Definition of reaction processes	4
2.2	Comparison of fusion cross sections	7
3	Experimental investigations	8
3.1	<i>Techniques</i>	9
3.1.1	<i>Identification of evaporation residues</i>	10
3.1.2	<i>Fission</i>	11
3.2	<i>Identification of reaction processes</i>	12
3.3	<i>Results of measurements</i>	13
3.3.1	${}^6\text{He} + {}^{64}\text{Zn}$	13
3.3.2	${}^6\text{He} + {}^{206}\text{Pb}$	15
3.3.3	${}^6\text{He} + {}^{209}\text{Bi}$	15
3.3.4	${}^6\text{He} + {}^{238}\text{U}$	17
3.3.5	${}^7\text{Be} + {}^{238}\text{U}$	18
3.3.6	${}^{10,11}\text{Be} + {}^{209}\text{Bi}$	19
4	Theoretical models	20
4.1	<i>Methods</i>	20
4.2	<i>Some widely available coupled channels codes</i>	22
4.3	<i>Model calculations for breakup</i>	22
4.3.1	<i>Conditions for the breakup calculations</i>	22
4.3.2	<i>Results of breakup calculations</i>	23
4.4	<i>Transfer reactions and their effect on other reaction channels</i>	27
4.4.1	<i>Conditions for the transfer calculations</i>	28
4.4.2	<i>Validity of transfer calculations: comparison to experimental data</i>	28
4.4.3	<i>Results of calculations: effect of the couplings on fusion</i>	33
5	Discussion	34
5.1	<i>Comparison between experimental data and calculations: conditions</i>	35
5.2	<i>Results and discussion</i>	37
6	Conclusions	44

1 Introduction

Collisions between two heavy nuclei can lead to a variety of processes. In a semiclassical picture, it is customary to use the impact parameter, or relative angular momentum, to distinguish between *compound nucleus* reactions (fusion reactions) and *direct* reactions; the latter take place for values of the impact parameter corresponding to grazing trajectories, the former occur for more central collisions. In between, *deep inelastic* reactions show intermediate behaviour. The relative importance of the different mechanisms depends on a number of factors; among these, a very important rôle is played by the kinetic energy and its value with respect to the amount of Coulomb repulsion between the nuclei for a given trajectory (the “Coulomb barrier”). At relatively high energies with respect to the barrier it is possible to use geometrical models of the reaction process to provide independent descriptions

of individual mechanisms: for example, Glauber models [1] for direct reactions, the one-dimensional barrier penetration model for fusion [2].

When the kinetic energy is small compared to the Coulomb barrier height this independence no longer holds: the behaviour of a particular process can no longer be considered separately from the others. In scattering theory this is expressed by the concept of *coupling* of the different *reaction channels*. Formally, the total wave function of the scattering problem contains the entrance channel and all possible exit channels; the Hamiltonian connects these states by means of potential terms, for example potentials that can create an excitation. For small kinetic energies, the contributions of these terms become significant in the determination of the wave function of each channel. The effect of the couplings is well-established, and visible on both the elastic scattering [3] and fusion cross sections [4, 5]. In this review we investigate the effect of such couplings when one of the participants in the reaction is a light, unstable nucleus.

As recognized since the very first measurements in the mid-eighties [6, 7], light exotic nuclei have properties which influence the reaction mechanism. Even models for high energy collisions must take into account the cluster structure of these nuclei [8] and their extended mass distributions. At energies around the Coulomb barrier the couplings between the various reaction channels are expected to be particularly important. This derives from the fact that some direct channels may be enhanced due to the characteristics of these systems: for example, selected transfer channels may be favoured by large positive Q -values and the cluster structure of the exotic nucleus; a low breakup threshold may cause a large cross section for the breakup channel.

To test these conjectures, more than ten years were necessary in order to develop suitable beams of radioactive nuclei in the energy range of interest and the experimental techniques to deal with the very low currents of such beams. The first measurements of the fusion cross section with light unstable projectiles were made in the second half of the nineties. Great interest in the fusion reaction mechanism was driven by the prediction of a possibly exceptional enhancement at sub-barrier energies when using a halo nucleus as projectile. The large spatial extension of the neutron matter density would cause the strong interaction to set in at larger distances, reducing the effect of the Coulomb repulsion. In addition, for these nuclei special couplings would appear: the presence of a large part of the dipole strength at low excitation energy, possibly concentrated into a resonance, would favour the corresponding excitation channel. However, as the breakup threshold in halo nuclei is very low the effect of the breakup channel becomes crucial.

An intense debate arose about the possible effect of breakup, mainly due to the way the mechanism was described. A low breakup threshold implies that the Coulomb or nuclear interactions can easily split the exotic nucleus into its cluster components. In one picture [9], this would enhance the breakup probability and, in turn, hinder the fusion of the whole exotic projectile with the target nucleus, due to a decrease of the number of nuclei available for fusion. This point of view assumes a two-step mechanism, a position which has been strongly objected to by other authors on grounds that are well described for example in [10]. They argue that a decrease in the observed flux reflected from the entrance channel (i.e. a decrease of the elastic scattering due to breakup) does not imply a decrease of the flux available for fusion: the latter can in fact even increase, since the transmitted flux is determined by a different region of the potential (more inside the barrier) with respect to the reflected flux. The problem can be properly treated only in a full coupled-channels picture. In this picture, coupling to other reaction channels at sub-barrier energies would lead to an enhancement of the transmitted flux and thus of the fusion cross section. This is the equivalent, at the nuclear level, of the enhancement of the tunnelling probability due to the presence of additional degrees of freedom in a given system, as described for example in [11].

The quantum-mechanical scattering problem should indeed be treated in its totality, and the coupled channels method is directly derived from the Schrödinger equation related to the problem. However, the inclusion of couplings is not always straightforward, and this has been the reason behind the

formulation of alternative descriptions. The inclusion of the breakup channel represents a particular challenge. Breakup is essentially an excitation of the nucleus to an energy higher than the corresponding threshold; if the calculation treats it in the same way as an inelastic excitation to a bound state, it will indeed lead to an enhancement of the tunnelling probability. However, the excitation is into the continuum, in many cases not even to a resonance and thus with no well defined values for the energy or spin of the final state. The effect of such a coupling cannot be predicted *a priori*.

A method to calculate the fusion cross section including the effect of breakup in a coupled-channels picture has not yet been fully developed. In an attempt to improve our understanding of the problem, we shall investigate the effect of breakup as a function of threshold energy and the target nucleus on the elastic scattering, a problem for which a realistic treatment is available (the Continuum-Discretised Coupled Channels method, CDCC).

In addition to breakup, we shall devote our attention to transfer channels and their effects. These are also expected to be large for light exotic nuclei, and indeed have recently been measured to be so. Transfer channels can be taken into account when calculating fusion in a coupled-channels framework, thus a detailed investigation is in this case possible.

Experimental investigation of reactions involving light exotic nuclei has been largely limited to those systems having a halo structure, i.e. essentially ${}^6\text{He}$ and ${}^{11}\text{Be}$ as the other halo nuclei (e.g. ${}^{11}\text{Li}$ and ${}^{14}\text{Be}$) are not yet available as beams with sufficient intensity. The effects due to breakup and transfer channels should also be largest for halo nuclei, due to their very low breakup thresholds and cluster structures. Since we wish to base our conclusions on the available experimental results we shall therefore be mainly dealing with halo nuclei. We choose to compare the measured fusion cross sections with calculations made with a bare potential obtained by folding the densities of the nuclei, and formulate our observations in view of this comparison and the results obtained from the coupled-channels calculations. Also, we limit ourselves to the very light systems up to $Z = 4$.

The structure of the paper is as follows. In section 2 we give a short list of definitions for the processes and quantities of interest, with the intention of aiding the clarity of the exposition. Even though the scope of the definitions is limited to this paper, we believe that this is a first, necessary step in trying to solve some of the ambiguities in this field. We then explain why, for our discussion, we choose to compare the experimental data to a fusion calculation obtained using a bare potential. In section 3 we present the techniques used in measurements with light unstable nuclei, and review the results for those systems for which fusion has been measured. We then discuss the coupled-channels methods for calculation of the fusion and direct reaction cross sections, describing ways of including the breakup channel. We use these methods for a series of model calculations for breakup and its effect on elastic scattering, and transfer and its effect on fusion. The available experimental data are consistently compared with model calculations for fusion in section 5 and general deductions are drawn. Finally, our conclusions are summarised in section 6.

2 Definitions

2.1 Definition of reaction processes

Halo nuclei have exhibited remarkable features since the measurement of the total interaction cross section in 1985 [6, 7]. Characteristics such as cluster structures and weak binding energies suggested that reaction mechanisms which were either usually neglected in reactions involving “normal” nuclei or previously unsuspected could be important. Unfortunately, the terms chosen to designate such processes have not always been used in a consistent way by all authors. In addition, some processes are difficult to define unambiguously. This has led to a sometimes confusing situation in the current literature, and certain discrepancies in reported results may be connected with this problem.

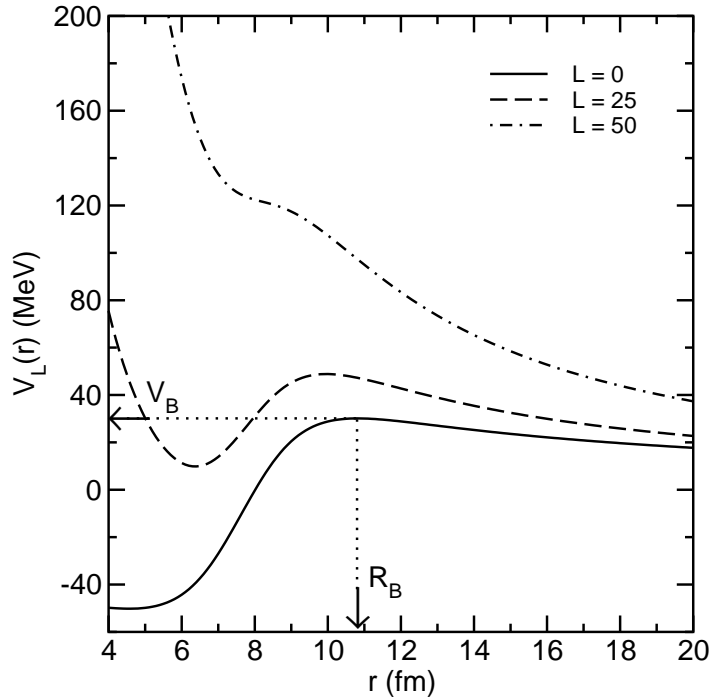


Figure 1: The interaction potential for ${}^7\text{Li} + {}^{208}\text{Pb}$ as a function of radial separation between the centres of the two nuclei for representative partial waves.

In this section we present a short list of definitions for use in the current paper. The aim is to adopt a uniform vocabulary in the review of experimental results and in the presentation of theoretical models, in order to facilitate comparison and help the clarity of the discussion.

- Coulomb barrier** The name given to the energy threshold that two nuclei must overcome in order to come close enough together to fuse classically. The Coulomb barrier (sometimes simply called the *potential barrier*) has a simple interpretation in the case of a one-dimensional potential, only depending upon the radial separation of the interacting nuclei. For a central collision the total potential is then given by the sum of the repulsive Coulomb and the attractive short-range nuclear potentials, see Fig. 1. The *barrier energy* is then the maximum of the combined potential, V_B , and its position is the *barrier radius*, R_B . For centre-of-mass collision energies lower than V_B fusion can take place only by quantum-mechanical tunnelling. If the collision is not central, the angular momentum contributes an additional centrifugal barrier. For large values of the angular momentum, the nuclear force is not sufficient to create a “pocket” and the potential is repulsive for all distances, see Fig. 1. Many results may be interpreted in terms of modifications to the height, position and shape of the barrier, due to the presence of strong direct reaction channels.
- Transfer** A rearrangement process whereby one or more nucleons are transferred from the projectile to the target nucleus or *vice versa*. A direct process, thus peripheral, taking place for angular momenta around the semiclassical critical value (corresponding to grazing trajectories). The resulting nucleus may be formed in its ground state or in bound or unbound (resonant) excited states. If formed in an excited state the residual nucleus may decay via the emission of γ rays (bound and some resonant states) or neutrons, protons or other charged particles (resonant states), or it may fission.

Transfer as intended here should be distinguished from the mass transfer occurring in *quasi-fission* processes [12]: the latter are heavy-ion dissipative reactions, in which exchange of nucleons leads to a deformed composite system which subsequently decays into fission-like fragments.

- **Breakup** A direct process where the projectile is split into two or more fragments, due to the Coulomb and/or nuclear interactions. A practical definition is the cross section obtained in a coincidence measurement, i.e. for the breakup process ${}^6\text{Li} \rightarrow \alpha + d$ the breakup cross section is defined as the $\alpha + d$ coincidence cross section. This definition thus excludes events where breakup is followed by capture of one or more of the fragments and is analogous to the definition of inelastic excitation of a bound excited state. We further restrict our definition to those coincidence events where the target remains in its ground state, corresponding to what is sometimes referred to in the literature as “elastic breakup”, the target nucleus remaining a spectator during the breakup process (see e.g. [13, 14, 15]).
- **Fusion** The process whereby two nuclei collide and coalesce to form a *compound system*. The term fusion is used to indicate any *compound nucleus process* between two heavy ions: the fusing nucleons lose the “memory” of the nucleus from which they came. Note that all the nucleons from both systems do not necessarily take part in the fusion process. The compound system initially has some excitation energy, and reaches equilibrium by emitting various kinds of prompt radiation: γ rays, light charged particles, neutrons, or possibly by fission. The heaviest remnant is the *residual nucleus*; this may in turn be unstable and emit further delayed radiation (α, β, γ) that can be detected for its identification.
- **Complete fusion** In this process, *all* nucleons from the projectile and the target fuse into the compound system. This quantity can be calculated by some models, but its unambiguous measurement is, in the general case, very difficult (see the discussion in section 3.2).
- **Incomplete fusion** This is the fusion of a large part of the projectile with the target nucleus. With light nuclei, for which only few nucleons are involved, incomplete fusion and transfer reactions remain conceptually different mechanisms but can lead to the formation of the same final nucleus in a similar excitation state. The angular momenta involved in the two processes are also similar, since the (semiclassical) value of the critical angular momentum is small. Thus, the separation between incomplete fusion and direct nucleon transfer may not even be significant experimentally, though attempts in this direction have been reported [16]. Incomplete fusion has been described in a two-step process picture as **fusion following breakup** where the projectile is first broken into two or more fragments by Coulomb and/or nuclear forces and some of the fragments penetrate the barrier and fuse with the target. Strictly speaking, events where *all* fragments fuse with the target nucleus after breakup are also possible (and experimentally indistinguishable from complete fusion). However, they must be considered as rather unlikely, although see [17]. In the introduction we discussed briefly the two-step picture as opposed to the coupled-channels one. In this respect, fusion following breakup should be distinguished from **sequential transfer** processes, which is the name given to those transfer probabilities which are coupled to an excitation to an unbound resonant state or the non-resonant continuum. Direct cluster transfer from the ground state of a light weakly bound nucleus can also produce the same residual nuclei as fusion following breakup and sequential transfer. Such processes need to be carefully distinguished from fusion events, see e.g. [18, 19, 20] and the discussion in section 3.2.
- **Total fusion** This is the sum of complete fusion and incomplete fusion. The complete projectile or one or more fragments fuse with the target. In many cases this is the simplest process to measure, as it is an inclusive cross section.
- **Fusion enhancement or suppression** There are two main schools of thought in the literature as to how to define whether fusion — in particular sub-barrier fusion — is enhanced or suppressed. The original definitions, used for stable, well bound heavy ions, were based on the observation that at sub-barrier energies the measured fusion cross sections were considerably larger than

those predicted by simple barrier-penetration type calculations using “standard” potentials that well described fusion above the barrier, see e.g. [21, 22]. Enhancement or suppression of fusion is therefore defined relative to the single barrier penetration model calculation prediction using some “reference” potential, derived either from a fit to the above barrier fusion cross sections or from a double-folding type calculation. Some more recent examples directly relevant to weakly bound nuclei may be found in e.g. [23, 24, 25]. The second school of thought compares the fusing system of interest either with some “reference” system that forms the same compound nucleus in complete fusion or the fusion of some “reference” nuclide with the same target, see e.g. [26]. In this review we shall define fusion enhancement or suppression relative to a barrier penetration calculation with a “bare” potential of double-folding type using realistic matter densities. These densities are the critical ingredient in the definition of the potential. Reasons for this choice and the difficulties associated with it will be discussed below.

We mentioned that there are a number of cases where the exact definition of a process is ambiguous. The choice of nomenclature may be more than mere semantics, as it implies the choice of a reaction mechanism with all that this entails when one attempts to simulate a given process theoretically. We have already discussed the important examples of incomplete fusion, fusion following breakup and sequential transfer. As another example, breakup may be thought of as a particular case of transfer, i.e. that of “transfer to the continuum”. For example, the transfer process: ${}^A\text{X}({}^{11}\text{Be}, {}^{10}\text{Be})\{{}^A\text{X} + n\}$ to the $n + {}^A\text{X}$ continuum of ${}^{A+1}\text{X}$ is equivalent to (and indistinguishable from) the breakup process: ${}^A\text{X} + {}^{11}\text{Be} \rightarrow {}^{10}\text{Be} + n + {}^A\text{X}$. See [27] for a full discussion of this point. However, reactions leading to ${}^{A+1}\text{X}$ final states that are distinct, narrow $n + {}^A\text{X}$ resonances are more naturally considered as conventional transfer reactions.

These ambiguities in choice of nomenclature can lead to confusion, as the same measured quantity may be referred to by two or more different labels that imply different production mechanisms. We have attempted to provide practical working definitions of quantities which can be measured in the ways discussed in sections 3.1 and 3.2; precise theoretical definitions of quantities that cannot be unambiguously measured are of little value. One is continually faced with the problem that when considering fusion induced by weakly bound nuclei those quantities that are most easily measured are most difficult to calculate theoretically and *vice versa*.

2.2 Comparison of fusion cross sections

A fundamental problem in choice of nomenclature concerns the definition of enhancement or suppression of fusion. We have already alluded to the two main schools of thought concerning this question, and it is by no means obvious that the different definitions will lead to similar conclusions. In posing the question as to whether fusion is enhanced or suppressed it is crucial to define the reference with respect to which the enhancement or suppression is to be judged. Both definitions have problems.

Taking our adopted procedure first, defining fusion enhancement or suppression relative to a single barrier penetration calculation, the main problem concerns the choice of reference potential. This has often been taken to be an energy-independent Woods-Saxon form, parameterised to fit the fusion cross sections well above the average barrier. However, it has been shown that the parameters of such potentials differ considerably from those obtained from fits to elastic scattering data [28], suggesting that the Woods-Saxon form may be inadequate. Also, coupling effects may still be significant even at energies well above the barrier and if these couplings are not explicitly included in the fitting procedure the fitted “empirical” bare potential will reflect this omission. Therefore, we prefer to employ a double-folded “bare” potential for these comparisons, although this does introduce its own set of problems through the choice of effective nucleon-nucleon interaction and matter densities, particularly when exotic nuclei are concerned.

The second approach, the comparison of the fusion excitation function of interest with that for a “reference” system, either one forming the same compound nucleus in complete fusion or one where a “reference” projectile fuses with the same target, has a different set of problems. The first concerns the removal of the “trivial” dependence of fusion cross section on the Coulomb barrier height and the size of the fusion partners. For the comparison of fusion involving similar stable, well-bound nuclei methods of “reducing” the fusion cross section to remove these geometric dependencies were evolved, see e.g. [29]. The reduction process involves dividing the measured fusion cross sections by the quantity πR_B^2 , where R_B is the barrier radius obtained from a fit to the fusion data at energies well above the Coulomb barrier and plotting the result as a function of $E_{c.m.}/V_B$, where V_B is the Coulomb barrier height, obtained from the same fitting procedure as R_B . This procedure, although inherently model-dependent, was found to give results relatively independent of the method used to extract V_B and R_B [29]. However, it may no longer be valid when applied to fusion involving halo nuclei which have much larger radii than normal nuclei of similar masses. A new procedure has been proposed to overcome this difficulty [30] which leaves a residual “geometrical” dependence due to the halo intact.

The main problem with this approach for weakly-bound halo nuclei, apart from the choice of reference system — should one compare with the fusion of the “core” nucleus with the same target or with the fusion of two well-bound stable nuclei forming the same compound nucleus in complete fusion — is that if enhancement or suppression of fusion is observed to occur there is no real clue as to the process or processes that cause it. To take a concrete example, suppose that the fusion of ${}^6\text{He}$ with ${}^{208}\text{Pb}$ at sub-barrier energies is observed to be enhanced with respect to that for ${}^4\text{He} + {}^{208}\text{Pb}$. Leaving aside the question of how best to “reduce” the cross sections to arrive at this conclusion, it is by no means clear in such a comparison whether this enhancement has been caused by coupling to the breakup of ${}^6\text{He}$ or by coupling to transfer reactions such as ${}^{208}\text{Pb}({}^6\text{He}, {}^5\text{He}){}^{209}\text{Pb}$ or ${}^{208}\text{Pb}({}^6\text{He}, {}^4\text{He}){}^{210}\text{Pb}$. It is mainly for this reason that we prefer to adopt a definition of enhancement or suppression of fusion relative to a single barrier penetration calculation with a “bare” potential; one can, in principle, explicitly include couplings to the processes of interest via the coupled-channels technique to investigate directly their effect on fusion relative to the reference calculation.

We have dwelt at some length on the question of a reference with respect to which enhancement or suppression of fusion may be defined as the use of different definitions in the literature has been a major source of the confusion in this area. In the next section we present a review of the experimental techniques used in the measurement of cross sections with beams of light unstable nuclei and the corresponding experimental results.

3 Experimental investigations

Experimental investigation of reactions involving halo nuclei has only become possible in the last two decades with the availability of radioactive ion beams. The results obtained so far are affected by the characteristics of these beams. The first experiments involving halo nuclei were performed with beams produced with the in-flight separation technique [31], at energies of some tens to several hundreds of MeV per nucleon; in addition to the low intensities, these beams often contained impurities in large quantities. In some favourable cases it was possible to slow down these beams, reaching energies around the Coulomb barrier [32]. However, most measurements in this energy region have been carried out since radioactive beams became available at Isotope-Separation-On-Line (ISOL) facilities [31] like the Cyclotron Research Centre (CRC) in Louvain-la-Neuve [33], GANIL-SPIRAL [34] and DUBNA-DRIBs [35]. Another method employs the separation of reaction products on a light target by means of magnetic fields produced by solenoids, and has been successfully implemented at the TwinSol facility at the University of Notre Dame [36, 37, 38] and more recently at the RIBRAS facility at the University of São Paulo [39].

The ISOL method provides pure beams of relatively good optical quality, although the intensities achievable with radioactive species are very low when compared to stable beams. Average intensities at the facilities mentioned above are of the order of 10^5 - 10^7 particles per second (pps). This fact has several consequences for the quality of the measurements.

A first obvious problem is the limited precision of measurements, since often only poor statistics can be collected. Another problem concerns the measurement of the beam intensity: on the one hand the currents are too low to be measured in a conventional Faraday cup, while on the other hand it is not possible to count the individual particles in beam detectors since the latter are very soon limited by saturation. The beam intensity is one of the factors that determine the data normalisation, together with the target thickness and the efficiency and accuracy of the detection method. Systematic errors can therefore be introduced, and special care needs to be taken to minimise this possibility.

If the elastic scattering is measured, a normalisation for the beam charge and target thickness can be derived from the forward-angle data, where the elastic cross section at energies around the Coulomb barrier follows the Rutherford formula. However, if the interest lies in other reaction channels the detection setup will not be optimised for elastic scattering; in addition, the efficiency of the detection will be different for elastic scattering and the process of interest and this has to be taken into account.

For fusion, one common practice has been to measure the cross section up to energies sufficiently high above the barrier that most calculations predict essentially identical fusion cross sections and to normalise the experimental results to these theoretical values. Another possibility is to measure, using the same setup and in the same conditions as with the radioactive isotope (weak beam intensity), the cross section for a nearby stable nucleus for which the above barrier fusion cross section may be calculated with more confidence. Conclusions have also been derived in some cases from a direct comparison of the experimental results for unstable and stable nuclei (see however the discussion in section 2.2).

A further aspect is the measurement of excitation functions (cross section values at several beam energies). With weak radioactive beams the number of different energies where measurements are carried out is limited by the time necessary to collect sufficient statistics. In addition, radioactive beams produced with the ISOL method are usually post-accelerated by cyclotrons as this provides the best possibility for beam purification (this is the case at CRC, SPIRAL, and DRIBs); however, changing the final beam energy takes considerably longer with a cyclotron than, for example, a linear accelerator. To partially compensate for the weak beam intensity thicker targets may be used; however, the corresponding energy loss of the beam in the target should be limited (and well-known) to retain a good definition of the actual energy of the projectiles inducing the reaction.

For the reasons listed above, it is clear that the quality of data collected using unstable beams cannot approach that obtained with intense stable beams. Various methods, which we describe in section 3.1, have nevertheless been used to tackle the different problems.

Directly connected to the detection method is the issue of the identification of the reaction process: using the list presented and discussed in section 2 as reference, we shall see that, experimentally, it is difficult to separate the contributions from different processes and a comparison with calculated cross sections can only be made with great care. We come back to this issue in section 3.2, after a discussion of the experimental techniques.

3.1 *Techniques*

Due to the low intensity of radioactive ion beams, experimental methods have necessarily focused on the efficiency of the detection setup: mostly, large detector arrays have been employed to maximize angular coverage, in combination with efficient signatures for the process of interest.

The measurement of elastic scattering is facilitated by its being the predominant process at energies around the barrier, at least at forward angles. The integral of the elastically scattered particles is

usually easy to evaluate. However, good angular resolution is necessary for the measurement of an angular distribution. To measure breakup, particle identification is necessary. This requires a more sophisticated setup, and only a few measurements have so far been performed with exotic nuclei.

For fusion processes the choice of the target is crucial to ensure an efficient signature. The latter is determined by the way the compound nucleus formed in the fusion process de-excites; however, it is rarely exclusive of a particular reaction process, so that inclusive cross sections are often measured. This fact represents a major problem and has eventually been the source of sometimes contradictory conclusions. The latest experiments address this issue, attempting to measure exclusive cross sections for a particular system.

The way compound nuclei de-excite depends upon their mass; since we consider here only light projectiles with masses up to $A = 11$, the detection method is determined by the choice of the target. De-excitation may take place by charged-particle or neutron evaporation, or by fission for the heaviest systems. The different possibilities may also be present together. Evaporated particles cannot be used to unequivocally identify the reaction channel, thus their detection is not crucial. In turn, the excited residue can be identified through its direct γ -ray emission and/or, when its ground state is unstable, through the detection of the characteristic decay radiation. In the following we discuss the various possibilities in more detail.

3.1.1 Identification of evaporation residues

After the possible evaporation of neutrons and/or charged particles, residues may emit different kinds of radiation (mostly depending on their mass) with different half-lives; this determines the setup used for the identification. From the number of detected decays (or decay chains), the cross sections in all evaporation channels have to be determined, then summed together to obtain the fusion cross section. If some channels are not measured, it may be necessary to rely on evaporation codes to extrapolate the respective cross sections; this is often the case when a residue is stable against β - or α -emission.

The activity per unit mass induced in the target is a combination of the irradiation time and the half-life of the residue. Short half-lives (up to a few seconds) require an on-line setup and a pulsed beam, with periods of the same order of magnitude as the half-life. Separate runs may be required to measure different isotopes, thus increasing the total time needed for a measurement. If the half-life is longer (in excess of some minutes at least, but not longer than a few months at maximum), an off-line setup can be used, which is then free from the constraints imposed by the conditions around the target.

In both cases, normalisation can be difficult. Besides a good calibration of the detection efficiency it requires a *continuous* measurement of the beam intensity, to correctly determine the production rate of short-lived isotopes. Further aspects are discussed below for the various types of radiation.

- *Detection of α activity.* By using targets around the ^{208}Pb region, the evaporation residues decay via emission of α particles. Charged-particle detectors are used to measure the energies; their characteristic values can be used, together with the half-lives, to determine precisely the number of decays of each isotope. Correlations in decay chains help in the evaluation. The different half-lives of the isotopes in the various channels may require both on-line and off-line measurements. This method has been applied to ^6He (see section 3.3.3) and ^{11}Be (section 3.3.6) induced fusion.
- *Detection of X-ray activity.* With an appropriate choice of target (stable, but proton-rich), the evaporation residues are unstable against β^+ -decay and electron capture (E.C.). If the latter process takes place, X-rays are emitted in the rearrangement of electrons in the shells; they are characteristic of the element and thus identify the charge number Z . The contributions of different isotopes can, in favourable cases, be disentangled by following the time behaviour of an X-ray line and fitting it using the known half-lives. These half-lives are mostly of the order of minutes or longer. Appropriate Si(Li) detectors can be used in an off-line setup, where X-rays

can be detected with 100 % intrinsic efficiency and extremely low background. The normalisation has to take into account the self-absorption of X -rays in the target; in addition, the geometrical efficiency of detection can be sensitive to the distribution of the activated nuclei in the targets. This technique was used for the first time with a radioactive beam in the measurement of ${}^6\text{He}$ on ${}^{64}\text{Zn}$, see section 3.3.1.

- *Detection of in-beam γ -rays.* The characteristics of this method have been described in [40]. The residues are identified through the emission of γ -rays corresponding to transitions between states. The main advantage of this technique is the fact that a residue does not need to be unstable against β - or α -decay; all evaporation channels can be directly investigated. To determine the total number of residues produced in a certain channel, all transitions from low-lying states are usually considered; extrapolations may be necessary to reconstruct the population of the $J = 0$ ground state when the energy of the transition is too low in even-even nuclei. A correction for the direct production of residues in their ground state may also have to be taken into account. However, usually the target nuclei are chosen such that this correction is negligible. To properly reconstruct the decay patterns a solid knowledge of the decay scheme of all the nuclei involved is necessary. The method requires good resolution for the detection of γ -rays in order to correctly identify the transitions, thus the use of HPGe detectors. With radioactive beams where high efficiency is also important, the only measurement so far carried out employed the EXOGAM detector array at GANIL [20], where the residues produced in ${}^6\text{He} + {}^{63,65}\text{Cu}$, ${}^8\text{He} + {}^{63}\text{Cu}$ and ${}^6\text{He} + {}^{188,190,192}\text{Os}$ were measured at energies slightly above the barrier. An important issue for γ -ray measurements is background: for its reduction, a coincidence trigger is normally used, provided either by the beam accelerator or by ancillary detectors; the latter can be charged-particle detectors and measure direct reaction cross sections simultaneously.
- *Direct detection of evaporation residues.* If the target nuclei are of light or medium-mass, the residues may have enough forward momentum to escape the target, making direct detection possible. The residues can then be identified in charged-particle ΔE - E telescopes, in magnetic separators, or by measuring their recoil velocity. Only the first method has been used to date with radioactive beams: the ${}^{13}\text{N} + {}^9\text{Be}$ fusion cross section was measured at the CRC [41], identifying the residues in special monolithic silicon telescope detectors [42]. The small velocity of the recoils and the large momentum dispersion are the main obstacle for the use of magnetic separators behind the target.

3.1.2 Fission

If the compound nucleus has a large mass and is produced with an excitation energy approaching its fission barrier [43], fission becomes a possible de-excitation mode. The branching ratio is at maximum a few percent for systems like ${}^{6,7}\text{Li} + {}^{209}\text{Bi}$ at energies about 1.5 times the potential barrier. By using a fissile target like ${}^{238}\text{U}$, however, the fission barrier of compound nuclei is at an energy around $V_{\text{FB}} \simeq 6$ MeV only, and the fission probability becomes ~ 100 % for projectile energies close to the Coulomb barrier.

The two massive fission fragments are emitted back-to-back in the centre-of-mass reference frame; for light projectiles this approximately coincides with the laboratory frame. The large energy of the fragments (a few tens to a hundred MeV) allows them to escape the target foil; charged-particle detectors, covering a large fraction of the total solid angle around the target, are used to identify the fragments based on their energy and, possibly, by the coincident detection of both particles. The setup needs to be calibrated with a fission source to determine its geometrical efficiency, and a correction may have to be introduced to account for the forward momentum of the compound nucleus.

The fission cross section obtained in this way is an inclusive one, as fission can be induced not only by (complete and incomplete) fusion but also by direct processes like inelastic scattering and transfer, leading to an excitation of the residual nucleus above the fission barrier. It is then necessary to devise a means of separating the possible contributions if one wishes to draw conclusions about the fusion process.

3.2 Identification of reaction processes

We introduced and discussed in section 2 definitions of different reaction processes. These definitions are meant to provide a basis for comparison between different measurements and between measured and calculated quantities. We have already discussed some of the problems faced by calculations due to the different possibilities for simulating a process theoretically. Here we discuss the difficulties present on the experimental side.

Experimentally, the identification of a reaction process is provided by a *signature* (detection of a particle, radiation, coincident detection, and so on). The corresponding cross section may be *exclusive* if the signature is produced by a single process; otherwise we speak about an *inclusive* cross section. The characteristics of weakly bound nuclei, and in particular of halo nuclei, may be responsible for modifications to the probability of a particular process with respect to the behaviour of more strongly bound systems. If different processes are measured together in an inclusive cross section the differences may be washed out and the peculiar effects overlooked; the effect of a particular reaction mechanism could be erroneously attributed to a different process. It is therefore important to measure exclusive cross sections, even if this has only been possible in a few cases so far.

Elastic breakup (“breakup” according to our definition) is identified by the coincident detection of the fragments; the cross section can be obtained in a straightforward way, taking into account a correction for the detection efficiency. Care has to be taken in order to unambiguously identify the fragments.

For fusion events, the signatures used for identification are those related to the detection of evaporation residues or fission, as discussed respectively in sections 3.1.1 and 3.1.2. However, either method alone is not sufficient to separate different types of fusion; in fact these signatures are not even exclusive of total fusion, they rather provide inclusive cross sections as discussed below. Access to exclusive cross sections is possible in some cases through a careful analysis supported by theoretical calculations, in other cases only if further detection means are available to add information on the process. We explore the different cases below.

If the de-excitation mode of the compound nucleus is through evaporation, in principle it is possible to determine the *complete fusion* cross section by summing all the contributions from the different evaporation channels; that is, by counting the corresponding residual nuclei in each channel. However, the same nuclei may be produced by different processes, like transfer or incomplete fusion. This is particularly true when the target is a medium-mass nucleus, since evaporation of charged particles is important in that case. For heavy targets (for example Os, Bi, Pb) the main de-excitation mode is through evaporation of neutrons; however, identification may have to be based upon detection of daughters from the α -decay of the original residue, thus presenting the same problem.

A number of methods can be used to help evaluate which part of the detected production of a residual nucleus is due to evaporation from a particular compound system. The predictions of evaporation codes give a reliable estimate of the ratio between the different evaporation channels from a compound nucleus with a given excitation energy: if a different process gives an additional contribution to a particular channel, the comparison with such predictions will help to identify the discrepancy and correct for it. An additional contribution, if present, can also be recognized if the nucleus belongs to a decay chain where the production of the mother nucleus is also measured. Another technique has been applied to nuclei decaying by α -particle emission in [44]: the analysis of the shape of the peaks in the α spectrum

revealed at which depth the nucleus was implanted in the catcher foil, thus giving information about its original energy and, in turn, on the production process. Further methods require the coincident detection of more observables. Particles identified as emitted at the moment of the reaction can rule out complete fusion, if a safe separation between reaction products and evaporated particles can be achieved (for example, if the reaction products present a distinctive angular distribution). Information on γ -ray multiplicity (obtained using an efficient detector, for example a BGO array) gives an estimate of the average angular momentum [45], which can then be used to predict the relative population of the different evaporation channels [46].

Using the techniques described above, usually in combination, it is possible to obtain a measurement of the cross section for complete fusion¹. The cross section corresponding to the additional production of some residual nuclei is then attributed to other processes, like incomplete fusion and transfer reactions.

If the compound nucleus formed in the fusion reaction de-excites through fission, complete fusion events can be identified as those for which the two fission fragments are the only emitted particles. If other processes are capable of producing fission, separation is possible through the detection of the light quasi-projectile fragment that emerges from the reaction.

Further identification of these processes (incomplete fusion vs. transfer) is not trivial, and requires information about the status of the heavy product. For example, events where the latter is formed in a narrow resonant state may be attributed to transfer. As mentioned in section 2 when discussing “incomplete fusion”, it could be argued that in the case of light projectiles at energies around the Coulomb barrier a separation may not even be significant experimentally: the energetics of the two mechanisms are similar, as are the angular momenta involved (which amount to a few units only), leading to the same range of excitation energies for the heavy product. We have already pointed out that attempts at achieving a separation have nevertheless been reported for the system ${}^7\text{Li} + {}^{165}\text{Ho}$ [16].

3.3 Results of measurements

In this section we present the set of experimental results that we use for our discussion. It includes the data collected so far on light unstable nuclei, for which the fusion cross section around the Coulomb barrier has been measured. Results for “companion” stable nuclei, obtained in the same measurements, are also included. The data are ordered by increasing mass of the projectile and target, rather than in a chronological order. Our aim here is to describe what was reported by the authors in their work, along with their conclusions; to facilitate this task, original figures are used. We will undertake a comparative discussion of all the systems and draw general conclusions in section 5.

A more comprehensive compilation of recent results, also including stable nuclei, has been presented in a recent review by Canto *et al.* [47].

3.3.1 ${}^6\text{He} + {}^{64}\text{Zn}$

The ${}^6\text{He}$ beam available at the CRC in Louvain-la-Neuve [33] was used in a series of experiments to measure elastic scattering, direct reaction [48] and fusion [19] cross sections on a ${}^{64}\text{Zn}$ target. The same quantities were also measured using a ${}^4\text{He}$ beam in the same energy region.

Elastic scattering was measured with very good angular resolution over a large angular range, at $E_{\text{c.m.}} = 9$ MeV for ${}^6\text{He}$ and at $E_{\text{c.m.}} = 12.4$ MeV for both ${}^6\text{He}$ and ${}^4\text{He}$; the latter data are shown in Fig. 2a. The total reaction cross sections were extracted from the data in the three cases. At $E_{\text{c.m.}} = 12.4$ MeV the value for ${}^6\text{He} + {}^{64}\text{Zn}$ is larger than that for ${}^4\text{He} + {}^{64}\text{Zn}$ by a factor of 2.2 (see Fig. 2a). The largest part of the cross section was accounted for by events where an α particle was

¹In fact, the quantity defined in this way includes the fusion of *all* fragments following breakup, a process that cannot be distinguished experimentally from complete fusion, as we mentioned in section 2.

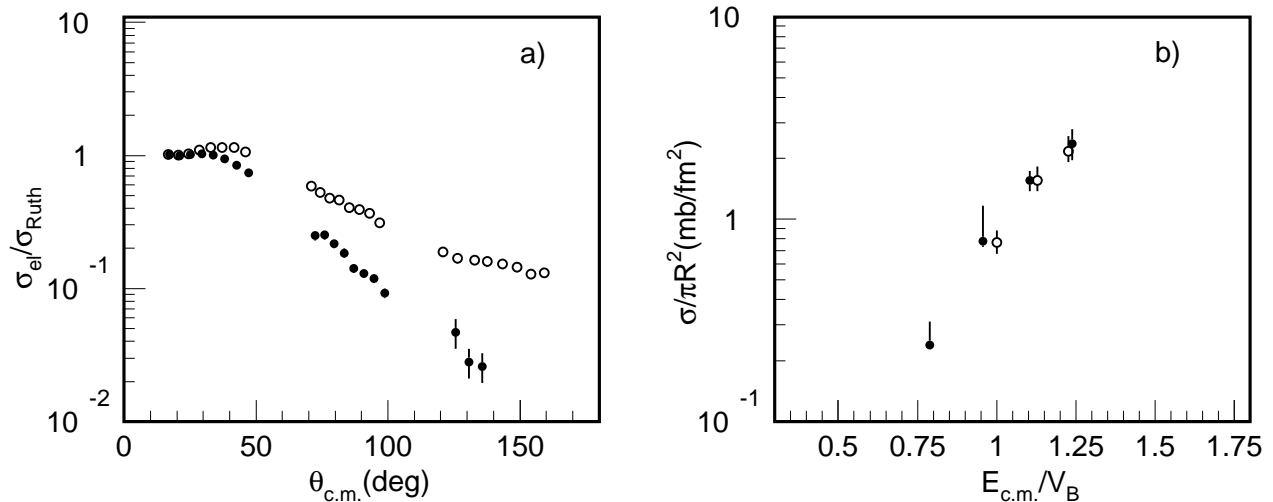


Figure 2: Results of the measurements for ${}^4\text{He} + {}^{64}\text{Zn}$ (open circles) and ${}^6\text{He} + {}^{64}\text{Zn}$ (filled circles): a) elastic scattering at $E_{\text{c.m.}} = 12.4$ MeV: the smaller elastic cross section for ${}^6\text{He}$ corresponds to a total reaction cross section a factor of 2.2 larger; b) fusion cross section normalised by the geometrical factor πR^2 , plotted as a function of $E_{\text{c.m.}}/V_{\text{B}}$. The values for ${}^6\text{He} + {}^{64}\text{Zn}$ have been corrected for the extra yield in the 1α - $1n$ evaporation channel. Figure adapted from [19].

emitted: $(79 \pm 29)\%$ at $E_{\text{c.m.}} = 9$ MeV and $(83 \pm 13)\%$ at $E_{\text{c.m.}} = 12.4$ MeV. An analysis of the angular distributions of the α particles from ${}^6\text{He}$ showed that most such events were due to direct reactions. From the information collected it was not possible to further distinguish between two-neutron transfer, one-neutron transfer and breakup reactions; however, an analysis of events where two charged particles were detected in coincidence showed that two-neutron transfer events were certainly present.

For the measurement of the fusion cross section the activation technique was used, with the detection of delayed X -ray activity emitted by the evaporation residues (see section 3.1.1). A stack of ${}^{64}\text{Zn}$ targets alternated with ${}^{93}\text{Nb}$ catcher foils was used; the latter increased the energy loss of the beam, differentiating the average irradiation energy for each Zn target. The residues in the various evaporation channels have half-lives between the hour and several months. Particular care was taken in order to control the uncertainties in the normalisation factors (detection efficiency, beam irradiation). The fusion cross section could be obtained by summing the yields of all evaporation channels; however, as discussed in the previous section, the same nuclei can be produced by fusion-evaporation and by direct reactions. In this case a comparison of the measured ratios between the different channels and a statistical model calculation showed a large discrepancy for the ${}^{65}\text{Zn}$ residue (1α - $1n$ evaporation channel). The excess in the yield measured for this channel was attributed to one- and two-neutron transfer reactions; the remainder is the *complete* fusion cross section.

Di Pietro *et al.* chose to compare the fusion cross sections for the ${}^6\text{He} + {}^{64}\text{Zn}$ and ${}^4\text{He} + {}^{64}\text{Zn}$ systems, plotted as a function of the ratio $E_{\text{c.m.}}/V_{\text{B}}$ and with the data points normalised by the geometrical factor πR^2 , where R is the sum of the projectile and target radii. Fig. 2b is reproduced from the original paper. The authors observed that the excitation functions are very similar and concluded that no sub-barrier enhancement of the fusion cross section is seen for ${}^6\text{He}$. They underlined instead the importance of direct channels, and remarked how the latter give a strong contribution in one particular evaporation channel, resulting in an enhancement of the total reaction cross section that could be misinterpreted as a fusion enhancement.

A new measurement has recently been performed [49], which extends the energy range of the excitation functions towards higher energies.

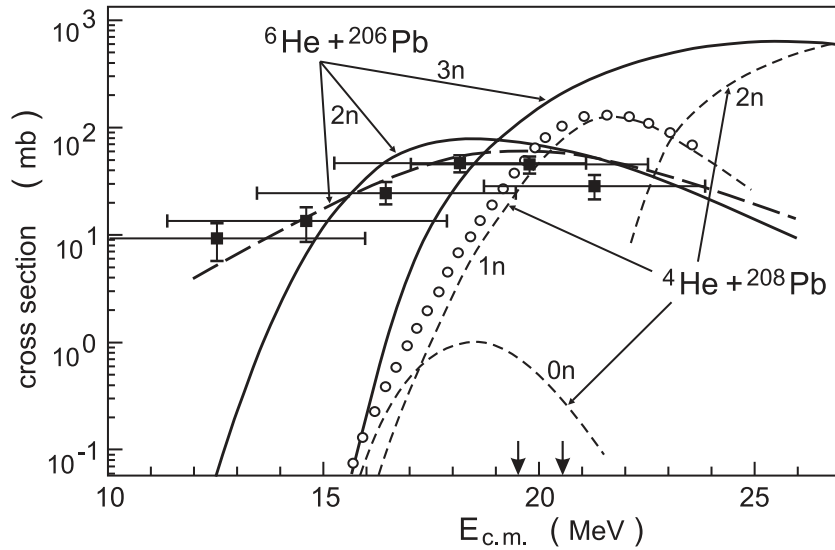


Figure 3: (taken from [50]) Cross sections for the production of ^{210}Po in the $^6\text{He} + ^{206}\text{Pb}$ reaction (solid squares) and for the production of ^{211}Po in the $^4\text{He} + ^{208}\text{Pb}$ reaction (circles). Dashed lines are predictions from a statistical model for the evaporation channels populated in $^4\text{He} + ^{208}\text{Pb}$. Solid lines are predictions from [51]; long-dashed lines take into account the energy spread. The arrows on the energy axis indicate the position of the Coulomb barrier for ^6He (left) and ^4He (right).

3.3.2 $^6\text{He} + ^{206}\text{Pb}$

Yu. Penionzhkevich *et al.* [50] measured the $^6\text{He} + ^{206}\text{Pb}$ system at the recently commissioned ISOL facility DRIBs [35] at the Flerov Laboratory in Dubna. The initial energy of the ^6He beam was $E_{\text{lab}} = 60.3$ MeV, thus degraders had to be employed to reach the energy range around the Coulomb barrier ($V_B \simeq 19$ MeV), resulting in a very large energy spread of the incident particles. A stack of ^{206}Pb targets was used, which allowed simultaneous measurements at different energies between 23 MeV and 13 MeV.

Results were reported for the two-neutron evaporation channel, measured using the activation method. The residual nucleus ^{210}Po decays emitting characteristic α particles at $E_\alpha = 5.3$ MeV with a half-life $T_{1/2} = 138$ d. The measured cross section data were compared with those for the 1n-evaporation channel in $^4\text{He} + ^{208}\text{Pb}$; both are shown in Fig. 3. The authors pointed to the large difference in the behaviour of the two cross sections at energies below the Coulomb barrier and concluded that there is a *large enhancement* of the fusion cross section for $^6\text{He} + ^{206}\text{Pb}$. In a model of “sequential fusion” proposed by Zagrebaev [51, 52], the transfer of the two “valence” neutrons in ^6He (with positive Q -value) would cause a gain in the energy of relative motion of the two nuclei and thus facilitate fusion: such a prediction was found to agree with the reported data (Fig. 3).

These experimental results are particularly surprising, as they show that at deep sub-barrier energies a sizable cross section is found. However, the large energy spread in these data, and the absence of a reference measured with the same experimental setup suggest that further investigation is necessary.

3.3.3 $^6\text{He} + ^{209}\text{Bi}$

The reaction channels in the $^6\text{He} + ^{209}\text{Bi}$ system were studied in a series of measurements at the TwinSol facility at the University of Notre Dame [36, 37, 38]. Two superconducting solenoids were used to separate and focus the nuclei produced in reactions on thin targets. For ^6He , a ^7Li primary beam was used with a ^9Be target. One concern of this technique is represented by contaminants in the

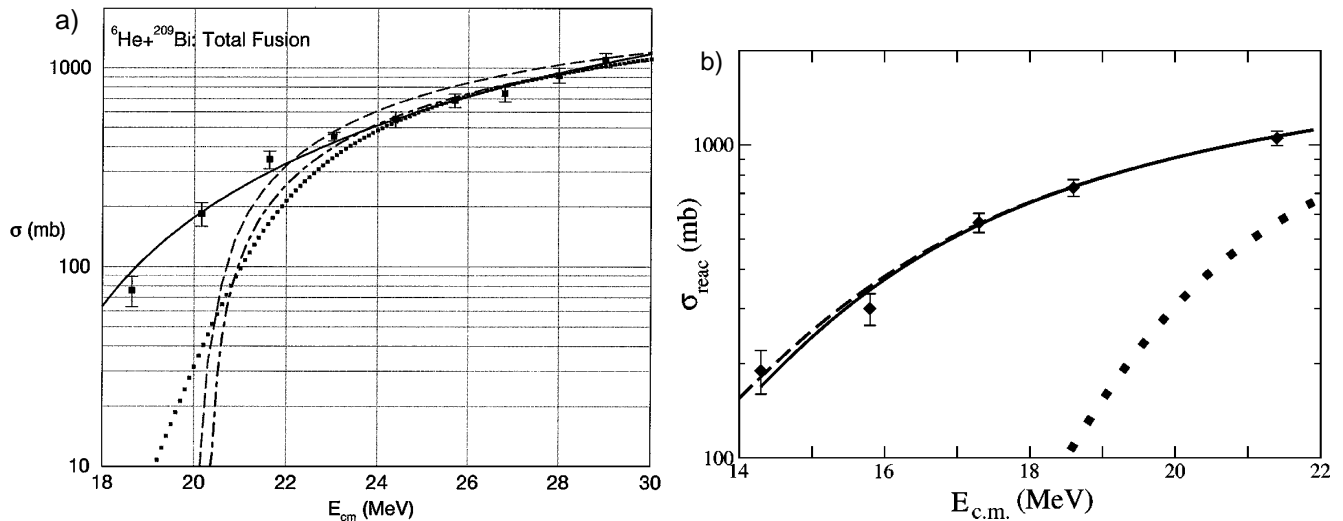


Figure 4: a) (from [24]) ${}^6\text{He} + {}^{209}\text{Bi}$ total fusion cross section; the dashed curve is the prediction of a statistical model, the dotted curve is a pure barrier penetration calculation, the dot-dashed curve is a $1/E_{c.m.}$ fit to the high-energy data and the solid curve is a fit according to the Stelson model [59]; b) (from [55]) total reaction cross section for ${}^6\text{He} + {}^{209}\text{Bi}$; the solid and dashed curves are calculations using parameters obtained from optical model fits to the elastic scattering data; the dotted curve is a prediction for the well-bound nucleus ${}^7\text{Li}$ on ${}^{208}\text{Pb}$.

beam, which have to be eliminated or identified; various methods were developed in the course of the measurement campaign to reach this goal.

The set of cross sections reported by the Notre Dame group is the most complete for this kind of system. It includes fusion-fission [53], the 4n evaporation channel [54], the 3n channel [24], elastic scattering [55], the total ${}^4\text{He}$ -production at near-barrier [56] and sub-barrier [55] energies, the 1n- [57] and 2n-transfer channels [58].

For fusion at energies in the vicinity of the potential barrier, the 3n and 4n evaporation channels are the most important. They were measured using the activation technique, detecting the α particles emitted in the on-line and off-line decay (3n and 4n channel, respectively) of the evaporation residues. In [24] the sum of the two cross sections is compared to a statistical model calculation and to a simple barrier penetration calculation, resulting in the plot reported in Fig. 4a. The plot also presents the result of a fit meant to determine the position of an effective barrier according to the “neutron flow” phenomenological model of Stelson *et al.* [59]. From their results, the authors concluded that there is an enhancement of the *total* fusion cross section at energies below the barrier and noted the good fit provided by the Stelson model; the model is related to the low-binding energy of neutrons in the projectile and thus transfer channels with positive Q -values, as in the case of the ${}^6\text{He} + {}^{209}\text{Bi}$ system.

Of particular interest is the observation of a large yield for α particles [56], exhausting the total reaction cross section resulting from optical model fits to the elastic scattering [55] (similar to that observed for ${}^4\text{He} + {}^{64}\text{Zn}$). The total reaction cross section is shown in Fig. 4b. In [58] at least 55% of this yield is attributed to the 2n-transfer channel to unbound states in ${}^{211}\text{Bi}$.

It has to be mentioned that the ${}^6\text{He} + {}^{209}\text{Bi}$ system has also been measured at the Flerov laboratory in Dubna at energies above the potential barrier ($E_{c.m.} = 25$ to 30 MeV), using a ${}^6\text{He}$ beam produced with the in-flight separation technique. Cross sections for fission and the 4n evaporation channel were reported [60, 61, 62]; the former was found to be a factor 3 to 4 larger than the corresponding ${}^4\text{He} + {}^{209}\text{Bi}$ cross section, however the large uncertainties at the lower energies ($E_{c.m.}$ smaller than 35 MeV) prevented firm conclusions. These results were not confirmed by the measurement of Kolata *et al.* [53], where the cross section at the same energy was reported to be about an order of magnitude smaller.

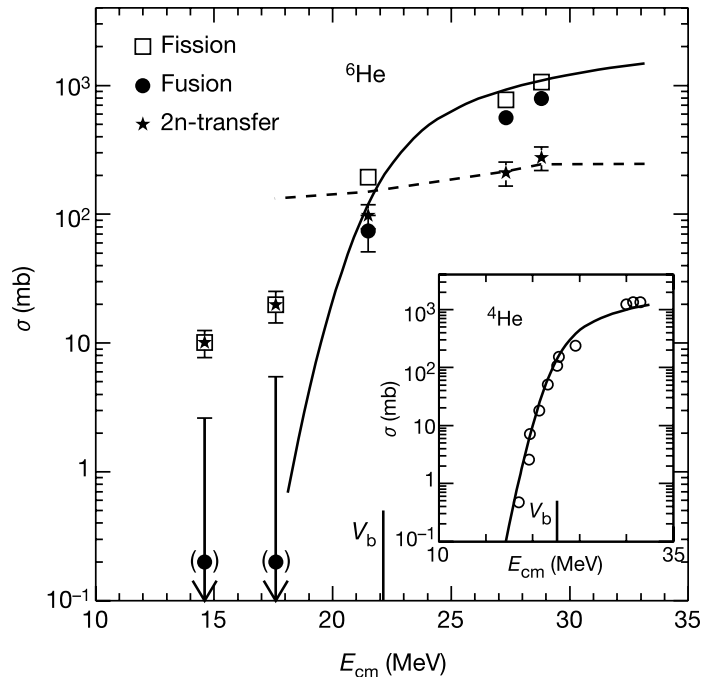


Figure 5: (from [18]) Cross sections for ${}^4,{}^6\text{He} + {}^{238}\text{U}$. The data are compared with calculations using an effective optical potential, which for ${}^6\text{He}$ was derived from a continuum discretised coupled channels (CDCC) calculation. The solid curves are fusion calculations using a short-ranged imaginary potential; the dashed line is the 2n-transfer cross section to excited states in ${}^{240}\text{U}$.

3.3.4 ${}^6\text{He} + {}^{238}\text{U}$

In these measurements, fission was chosen as the signature to identify fusion. The nuclei in the region around ${}^{238}\text{U}$ have low fission barriers, $V_{\text{FB}} \simeq 6$ MeV [43]. For projectile energies around the potential barrier ($V_{\text{B}} \simeq 21$ MeV for ${}^6\text{He}$ and $V_{\text{B}} \simeq 23$ MeV for ${}^4\text{He}$), a fusion reaction will always produce a compound nucleus at an excitation energy well above the fission barrier inducing a fission probability close to 100%.

This measurement, like the one on ${}^{64}\text{Zn}$, was performed using the ${}^6\text{He}$ beam at the CRC in Louvain-la-Neuve. To attain a large efficiency for the detection of the two fission fragments, forty large-area charged-particle silicon detectors were placed on the inner surfaces of two cubes, symmetrically arranged around the target position, covering about 70% of the whole solid angle.

As explained in section 3.1.2, other reactions besides fusion are capable of exciting the target nucleus above its fission barrier. In these cases, however, a quasi-projectile fragment would be emitted in the process and, if charged, could be detected in coincidence with the fission fragments (a correction for the geometrical efficiency for the detection of the quasi-projectile particle needs to be included). With beams of He isotopes, the capture of the whole charge of the projectile would very likely correspond to *complete* fusion — the only other possibility, very unfavourable energetically, being for ${}^6\text{He}$ the transfer of the α particle core. The results were published in [63, 18], and they are summarised in Fig. 5 (taken from [18]). The authors compared the behaviour of the two isotopes: the fission cross section for ${}^6\text{He} + {}^{238}\text{U}$ shows an enhancement at energies below the barrier with respect to ${}^4\text{He} + {}^{238}\text{U}$ and also with respect to ${}^6\text{Li} + {}^{238}\text{U}$ (the data for ${}^6\text{Li}$, from [64], are not shown in the figure). However, for ${}^6\text{He}$ most of these fission events were not due to fusion, as revealed by the detection of a quasi-projectile particle in coincidence. Once this contribution was subtracted, only upper limits for the complete fusion cross section could be given for the two points measured below the barrier, and the conclusion was that no enhancement was observed. The process generating the large fission yield was identified through an

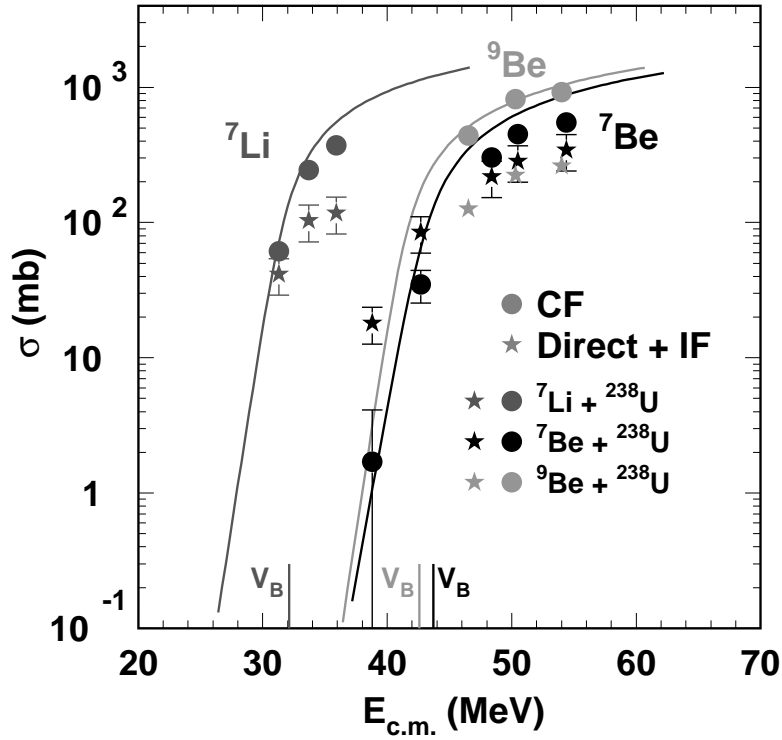


Figure 6: (from [65]) Cross sections for complete fusion (filled circles) and incomplete fusion (IF) + direct processes (stars) for ${}^7\text{Li}$, ${}^7\text{Be}$ and ${}^9\text{Be}$ on ${}^{238}\text{U}$. Curves are one-dimensional barrier penetration model calculations for fusion.

analysis of the energies and angular distributions of the quasi-projectile particles to be the transfer of two neutrons to the target to form ${}^{240}\text{U}$. The optimum matching conditions favour transfer to excited states of ${}^{240}\text{U}$ above the fission barrier. Taking into account that direct breakup could not be measured due to the required fission signature, the observation of a large reaction cross section for direct reactions at energies below the barrier is similar to that reported for ${}^6\text{He} + {}^{64}\text{Zn}$ and ${}^6\text{He} + {}^{209}\text{Bi}$.

3.3.5 ${}^7\text{Be} + {}^{238}\text{U}$

The ${}^7\text{Be}$ nucleus is unstable and relatively weakly bound (the lowest breakup threshold is that into $\alpha + {}^3\text{He}$ at $E^* = 1.59$ MeV). However, it does not exhibit a halo structure; we include it in this review to find possible differences with respect to halo nuclei.

The ${}^7\text{Be}$ beam was produced at the CRC in Louvain-la-Neuve from nuclei obtained from a (p,n) reaction on ${}^7\text{Li}$ and chemically separated off-line (the half-life of ${}^7\text{Be}$ is $T_{1/2} = 53$ d). The same fission signature technique described above was used; in the case of ${}^7\text{Be}$, in addition all possible fragments (α , ${}^3\text{He}$, ${}^6\text{Li}$, d, p) are charged and were thus detected. The *complete* fusion events can therefore be unambiguously identified as those fissions not accompanied by the emission of light particles. The results of this measurement appeared in [65], from which Fig. 6 is taken. The authors compared the cross section data for ${}^7\text{Be}$ with those for ${}^7\text{Li}$ and ${}^9\text{Be}$ on the same target. Their main conclusion was that the pattern is similar to that observed in the case of ${}^6\text{He} + {}^{238}\text{U}$: at energies below the potential barrier a large total reaction cross section is observed. However, this is mainly due to processes other than complete fusion, since a charged light particle was detected in coincidence. The sub-barrier complete fusion cross section for ${}^7\text{Be}$ does not differ much from a one-dimensional barrier penetration model calculation, and no enhancement was observed. At energies around and above the barrier, on the other hand, the fusion cross section is smaller than the calculation, and the authors speak of a suppression of

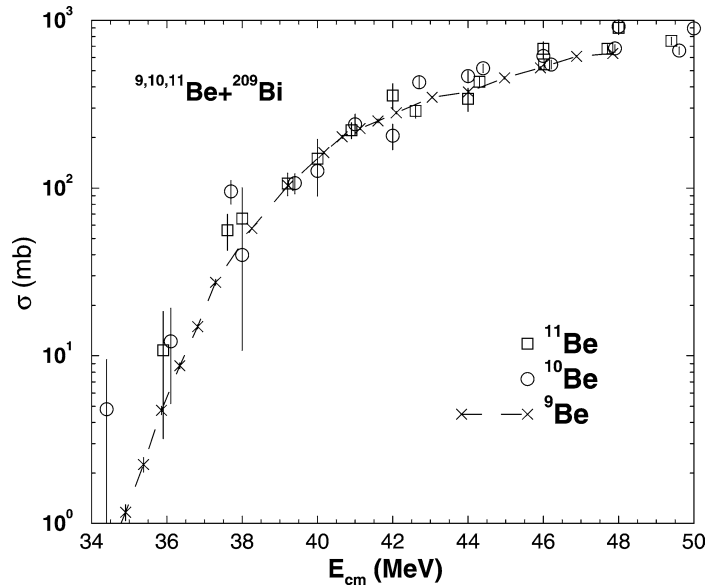


Figure 7: (from [67]) Fusion cross sections for the systems $^{9,10,11}\text{Be} + ^{209}\text{Bi}$.

the complete fusion. Concerning the nature of the processes generating the large fission cross section, it was suggested that they mostly consist of transfer of clusters to the target nucleus and possibly with a component due to reactions characterised by a small impact parameter and thus more properly labelled incomplete fusion.

3.3.6 $^{10,11}\text{Be} + ^{209}\text{Bi}$

The fusion cross sections for the $^{10,11}\text{Be} + ^{209}\text{Bi}$ systems were measured at RIKEN, Japan, using the target activation method in two successive experiments [66, 67]. The beams were produced using the in-flight separation technique; from an initial energy of about 45 MeV/nucleon, the Be nuclei were slowed down to energies around the potential barrier using thick degrader plates. While the energy spread of the beam was very large, for each nucleus impinging on a stack of targets the energy was determined using the time of flight, achieving an accuracy of about ± 1 MeV. Following activation, the short-lived ($T_{1/2} < 1 \mu\text{s}$) residual nuclei in the targets decayed emitting α particles. Given the short half-lives and the low beam rate, each decay could be correlated to a projectile of known energy, obtaining excitation functions for evaporation channels corresponding to the residual nuclei $^{215,216}\text{Fr}$ (5n and 4n evaporation channels for $^{11}\text{Be} + ^{209}\text{Bi}$).

The cross section data for the weakly-bound ($E_B = 0.50$ MeV) one-neutron halo nucleus ^{11}Be were compared with those for the well-bound ($E_B = 6.8$ MeV) ^{10}Be nucleus. In addition, the fusion of the stable but weakly-bound ($E_B = 1.57$ MeV) ^9Be nucleus with ^{209}Bi was measured by the same group at the Munich Tandem accelerator [68].

All these data are presented together in Fig. 7, taken from [67]. Those for ^{11}Be and ^{10}Be are total fusion cross sections, obtained as the sum of the measured evaporation channels; the authors argue that the incomplete fusion amounts to less than 30% for ^{11}Be and is negligible for ^{10}Be . For ^9Be , the data represent the complete fusion cross section. In the case of ^{11}Be (^{10}Be), the 3n (2n) evaporation channel is not included, which may lead to an underestimation of the cross section in the sub-barrier region; however, the effect should be comparable for the two systems. The main conclusion of the authors concerned the unexpected similarity between the three cross sections, while ^{11}Be was expected to show pronounced effects due to its weakly-bound nature; thus, they speak of neither enhancement nor hindrance of the fusion cross section for ^{11}Be . It was also correctly underlined that ^9Be , stable

but weakly bound, may not be a good reference system for comparison [69]. ^{11}Be and ^9Be also show comparable behaviour concerning elastic scattering, as recently reported by the same group [70].

With the review presented above, we wish to show how experimental investigations in this field face many challenges that may lead to uncertain results. In addition, by reporting the original remarks of the authors, it becomes perhaps more apparent how the sometimes contradictory conclusions may have originated from the different ways chosen to present those results.

In the next section we will perform calculations and analysis for those reaction mechanisms involving weakly bound nuclei that can be predicted with a good degree of confidence. From the results we will derive some conclusions about the expected behaviour of these nuclei at energies around the potential barrier. In section 5 we will then compare the experimental data presented here with a simple, consistent model, and try to draw some general conclusions about the possible effects of weak binding and transfers.

4 Theoretical models

In this section we present and discuss some of the theoretical models used to describe direct reactions and fusion at incident energies close to the top of the Coulomb barrier. These models are then used to investigate the effect of breakup and transfer couplings on other reaction channels for weakly bound nuclei.

4.1 *Methods*

It has been firmly established that strong coupling effects are important for both elastic scattering ([3] and references therein, see [71, 72, 73, 74, 75, 76, 77] for some recent examples with exotic nuclei) and fusion [4, 5] induced by heavy ions at incident energies close to the top of the Coulomb barrier. In particular, it was shown that under certain approximations the single fusion barrier could be thought of as splitting into a distribution of barriers when couplings to other channels are present. Calculations that explicitly include these couplings are able to satisfactorily describe the ensemble of nuclear reaction data in this energy regime, e.g. [78, 79, 80, 81, 82]. The standard coupled-channels (CC) techniques for the analysis of direct nuclear reactions are presented in a number of text books, e.g. Satchler [83], and will not be covered here. Similarly, there are a number of review articles discussing the analysis of near-barrier fusion data for stable, well-bound nuclei [4, 5, 84, 85, 86]. Attempts have been made to extend these standard techniques to enable the inclusion of breakup for both direct reactions and fusion, essential for detailed analyses of weakly-bound systems such as halo nuclei.

For the description of breakup and its effect on other direct reaction channels, most importantly the elastic scattering, the most sophisticated and successful theory currently available is incontestably the continuum discretised coupled channels (CDCC) method. An extension of the standard coupled channels theory to allow treatment of couplings to the unbound continuum of states above the breakup threshold, it was first developed to describe deuteron breakup [87] (see [88] for a recent systematic application to many target nuclei). The method was later extended to other weakly-bound systems; ^6Li [89], ^7Li [90] and ^7Be [91]. In particular, the continuum–continuum coupling, i.e. coupling between the “excited states” of the continuum, has been found to play an important rôle [92, 93]. Two comprehensive reviews of CDCC applied to deuterons [94] and other nuclei [90] provide numerous examples of its success. The formalism has been recently extended to include systems that break up into three particles [74, 77, 95] and to systems that include an “active” core [96, 97]. These extensions are essential for a realistic description of the breakup of weakly-bound halo nuclei.

Although CDCC has proved remarkably successful in describing breakup and its effect on other direct reaction channels, to date there is no completely satisfactory way of linking it to a calculation of fusion. A method has been proposed for calculating *total* fusion within the framework of standard

CDCC [98] by the use of short-ranged imaginary potentials for each of the two fragments, simulating the ingoing-wave boundary condition. These potentials are then folded together with the projectile internal wave functions to produce the final imaginary potentials. The total fusion is then defined as the amount of flux that leaves the coupled channels set, i.e. the total absorption cross section, obtained by subtracting the cross sections of all channels explicitly included in the coupling scheme from the total reaction cross section. However, unfortunately this technique cannot be used to calculate incomplete fusion as it is impossible to trace the trajectories of the individual fragments after breakup has occurred. Also, to describe the direct channels simultaneously with the fusion one would need to include many other channels, e.g. inelastic excitation of the target and transfers, and the couplings between them. Such calculations are not currently tractable for most systems, although this problem is a general one and not confined to this particular method.

Another, much more approximate way of calculating a fusion cross section within the CDCC framework is to employ a one-dimensional barrier penetration model (BPM) in conjunction with a dynamic polarisation potential (DPP) generated by the couplings to the continuum. The BPM assumes that all the flux that penetrates the Coulomb barrier, defined in this instance by the real part of the effective scattering potential, leads to fusion. As the real part of the DPP is energy dependent (particularly for energies close to the Coulomb barrier) this model replaces the distribution of barriers of the full coupled channels scheme with an energy dependent one-dimensional barrier. Although this method has been applied to fusion induced by weakly bound projectiles [99], it is not completely clear whether the calculated fusion cross sections should be compared with complete or total fusion measurements.

There are other problems with the CDCC+DPP+BPM approach, notably in the definition of the DPP which may be the “trivially equivalent local potential” (TELP), as used in [99] and based on wave functions, or a potential obtained by inversion of the S-matrix [100]. While both methods give the same elastic scattering for a given system it is by no means clear that they will give the same fusion cross section, as their radial forms are often very different in the nuclear interior. It has also been found that for well-bound nuclei the CC+DPP+BPM approach consistently underpredicts the fusion cross sections of the more realistic ingoing-wave boundary condition model [101].

Clearly, some means of linking the CDCC description of breakup to a realistic method of calculating fusion is required. In particular, a method that enables the trajectories of the fragments to be traced is needed if incomplete fusion — in this context fusion following breakup — is to be reliably calculated and separated (at least theoretically) from other processes yielding the same residual nuclei.

While breakup has excited the most interest among the reactions that may be induced by halo nuclei, due to their very low thresholds against this process, one should not overlook the possible importance of transfer reactions. The low one or two neutron removal energies of the halo nuclei should also favour neutron stripping reactions [57, 58]. A reliable model exists for the calculation of transfer processes in the coupled reaction channels (CRC) framework, an extension of the coupled channels formalism to include channels belonging to different partitions. The calculation of fusion is readily incorporated within the CRC formalism by using the ingoing-wave boundary condition [79, 102] or its equivalent [103]. In this case, the standard formalism developed for well-bound stable nuclei (see e.g. Satchler [83]) may be used without modification for halo nuclei, although care may be needed in the choice of bound-state form-factors in order to take account of the halo properties.

Although we shall not discuss them further here, we note that time-dependent wave-packet methods provide an alternative view of the fusion problem to that provided by the coupled channels scheme. A three-body model using this method has recently been applied to the fusion of neutron halo nuclei with heavy targets [104].

As a recent review article [47] has already provided an excellent summary of the considerable literature concerned with the effect of coupling to breakup on near and sub-barrier fusion, and owing to the lack of a theoretical model that treats fusion and breakup equally realistically, we shall not further investigate this subject here. However, we shall probe the influence of breakup threshold on the elastic

breakup cross section and the effect of breakup coupling on the elastic scattering through model calculations. We shall also investigate the effect of transfer reactions on fusion induced by weakly bound nuclei through CRC calculations comparing systems involving ${}^6\text{Li}$, ${}^6\text{He}$ and ${}^8\text{He}$ projectiles. Before doing so we shall briefly list in the next section some of the more widely available codes that are frequently used to perform coupled channels and coupled reaction channels calculations. Section 4.3 contains an investigation of the effect of breakup threshold energy on the total cross section for breakup and its influence on the elastic scattering while section 4.4 concentrates on the effect of transfer reactions.

4.2 *Some widely available coupled channels codes*

Some of the most frequently used coupled channels codes in the literature are ECIS [105], PTOLEMY [106], FRESKO [107] and CCFULL [108]. This list is not intended to be exhaustive, but merely indicative of the types of code available for coupled channels and coupled reaction channels calculations. ECIS, PTOLEMY and FRESKO are general reaction codes whereas CCFULL calculates the fusion cross section only. Brief descriptions of the capabilities of these codes follow.

- ECIS uses the full CC method to calculate inelastic excitations of target and projectile. Transfer reactions may be included via zero-range CRC and parameter searches to fit a set of experimental data are possible.
- PTOLEMY, like the previous code, calculates inelastic excitations using full collective model CC. Transfer reactions are included via the exact finite-range distorted-wave Born approximation (DWBA).
- FRESKO is a very complete code for the calculation of direct reactions. It uses full CC for inelastic excitations and transfer reactions are included via full finite-range CRC (implemented iteratively) with complex remnant term and non-orthogonality correction. Three-body breakup (i.e. breakup of one of the interacting partners into two fragments) may be included via the CDCC method employing Watanabe-type cluster folding. Parameter searches are possible using the auxiliary code SFRESKO.
- CCFULL focuses on the calculation of the fusion cross section. It can include inelastic excitations of both particles (rotational and vibrational couplings) and a transfer between ground states using a coupling form factor. The effect of couplings is taken into account to all orders. The barrier penetrability is calculated for each partial wave, and to obtain the fusion cross section the ingoing-wave boundary condition is used.

4.3 *Model calculations for breakup*

4.3.1 *Conditions for the breakup calculations*

In this section we use the CDCC method to probe the influence of breakup threshold and target charge, i.e. the magnitude of the Coulomb potential, on the total elastic breakup cross section and the effect of breakup coupling on the elastic scattering through a series of model calculations using the coupled reaction channels code FRESKO [107]. We employ a simplified “ ${}^7\text{Li}$ ” projectile with ground-state spin $0\hbar$, no resonant states and breakup thresholds set at 1.0, 1.5, 2.0 and 2.5 MeV. As targets, we take ${}^{208}\text{Pb}$, ${}^{58}\text{Ni}$ and ${}^{12}\text{C}$, as representative of systems where the Coulomb force is dominant (${}^{208}\text{Pb}$) through to those where the nuclear force predominates (${}^{12}\text{C}$). We employ a two-body $\alpha + t$ model of ${}^7\text{Li}$ with the triton spin set to $0\hbar$ and the $\alpha + t$ continuum discretised in the usual way [90] into a series of bins in momentum (k) space of width $\Delta k = 0.1 \text{ fm}^{-1}$ up to a maximum of $k_{\text{max}} = 1.0 \text{ fm}^{-1}$. The value of k_{max} was reduced for the lower incident energy calculations as required.

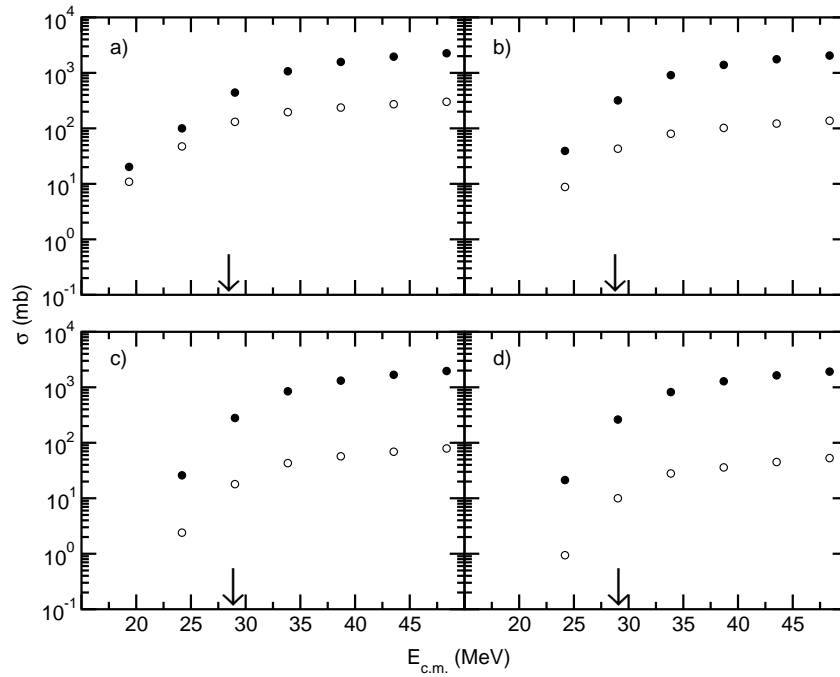


Figure 8: Model breakup calculations for a ^{208}Pb target with breakup thresholds of: a) 1.0 MeV, b) 1.5 MeV, c) 2.0 MeV and d) 2.5 MeV. The filled and open circles denote the total reaction cross section and total breakup cross section, respectively. The arrows indicate the positions of the respective Coulomb barriers, defined as the maximum of the combined bare nuclear plus Coulomb potentials.

All diagonal and coupling potentials were of the Watanabe cluster-folding type as in e.g. [109]. The α and triton plus target potentials required for the folding procedure were taken from [110] and [111], [112] and [113], [114] (potential III) and [115] for the ^{208}Pb , ^{58}Ni and ^{12}C targets, respectively. All these potentials are energy-independent, therefore the energy dependencies of the calculated cross sections are strictly dynamic, depending on the couplings alone.

4.3.2 Results of breakup calculations

The results are presented in Figs. 8–10 as excitation functions of total reaction cross section and total breakup cross section.

A number of observations are immediately apparent:

- With the exception of the results for a breakup threshold of 1.0 MeV and a ^{208}Pb target the total breakup cross section makes a small or negligible contribution to the total reaction cross section.
- The total breakup cross section is very sensitive to the breakup threshold for the ^{208}Pb target, less so for ^{58}Ni and ^{12}C , diminishing with increasing threshold energy, as might be expected.
- The behaviour as a function of energy of the ratio of total breakup cross section to total reaction cross section for the ^{208}Pb target differs from that for the ^{58}Ni and ^{12}C targets, i.e. for the ^{208}Pb target this ratio decreases as a function of increasing incident energy, whereas for the other two targets the reverse is true.

These results show that in terms of total cross section breakup is a *quantité négligeable*, except for heavy targets at incident energies close to or below the Coulomb barrier where the Coulomb force should dominate. In these “optimal” conditions the total breakup cross section is approximately 50% of the

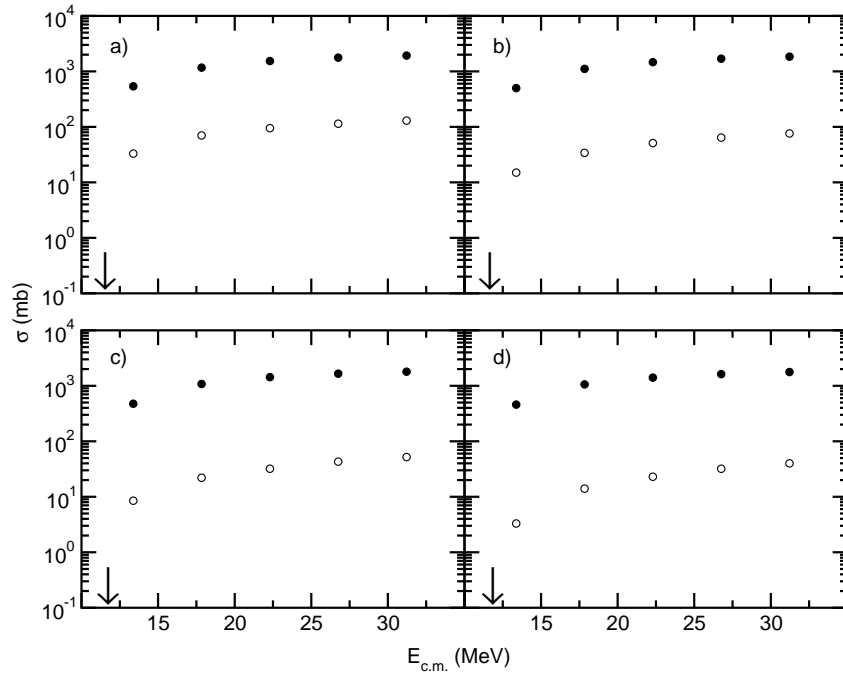


Figure 9: Model breakup calculations for a ^{58}Ni target with breakup thresholds of: a) 1.0 MeV, b) 1.5 MeV, c) 2.0 MeV and d) 2.5 MeV. The filled and open circles denote the total reaction cross section and total breakup cross section, respectively. The arrows indicate the positions of the respective Coulomb barriers, defined as the maximum of the combined bare nuclear plus Coulomb potentials.

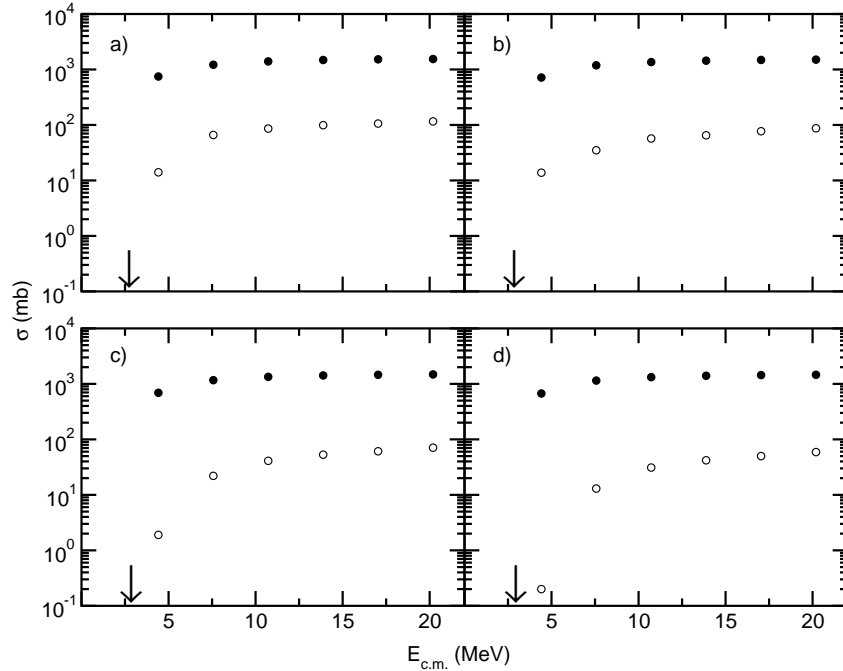


Figure 10: Model breakup calculations for a ^{12}C target with breakup thresholds of: a) 1.0 MeV, b) 1.5 MeV, c) 2.0 MeV and d) 2.5 MeV. The filled and open circles denote the total reaction cross section and total breakup cross section, respectively. The arrows indicate the positions of the respective Coulomb barriers, defined as the maximum of the combined bare nuclear plus Coulomb potentials.

total reaction cross section for the lowest breakup threshold (1.0 MeV) at an incident energy of 25 MeV, diminishing rapidly as the breakup threshold energy increases — it is of the order of 5% for a breakup threshold of 2.5 MeV under the same conditions. However, in general the magnitude of the cross section is not a reliable guide to the influence of a coupling on other channels, see e.g. [116, 117, 118]. Coupling to breakup is known to have an important effect on the elastic scattering, particularly for energies near the top of the Coulomb barrier, for a wide range of targets, see e.g. [90]. The first hint of this important effect came when the hitherto highly successful double-folding model potential [119] had to be renormalised by a factor of order 0.5 to fit elastic scattering data for the weakly-bound nuclei ${}^6\text{Li}$ [120], ${}^7\text{Li}$ [121] and ${}^9\text{Be}$ [122]. This renormalisation was subsequently shown to be due to a large positive real DPP produced by coupling to breakup [90, 123, 124, 125], although the propriety of simulating what is normally a surface-peaked DPP by a simple renormalisation of the whole potential is, to say the least, questionable, particularly if the same potential is to be used to calculate fusion within the one-dimensional barrier penetration formalism. However, CC calculations that adopted this procedure to simulate the effect of couplings to breakup that were not explicitly included in the coupling scheme proved remarkably successful in describing fusion data for systems involving weakly bound projectiles [126]. In fine, the relatively small cross section belies the importance of breakup in terms of its influence on other channels.

Before drawing conclusions from our calculations, we shall briefly show that although they have been considerably simplified they nevertheless produce qualitatively realistic results. Two recent coincidence measurements have been performed for the ${}^6\text{Li} + {}^{208}\text{Pb}$ [127] and ${}^6\text{Li} + {}^{28}\text{Si}$ [128] systems and total $\alpha + d$ breakup cross sections are reported. For the ${}^6\text{Li} + {}^{208}\text{Pb}$ system, the total breakup cross sections [127] at incident energies of 31 and 39 MeV provide approximately 8% and 5%, respectively, of the total reaction cross section derived from optical model fits [129]. For our simplified calculations presented in Fig. 8b this ratio is approximately 13% and 7% at similar incident energies for a breakup threshold of 1.5 MeV, close to the $\alpha + d$ threshold of ${}^6\text{Li}$. For the ${}^6\text{Li} + {}^{28}\text{Si}$ system, the ratio of measured total $\alpha + d$ breakup cross section to total reaction cross section at an incident energy of 13 MeV is approximately 2% [128]. Our simplified calculations for ${}^{58}\text{Ni}$ and ${}^{12}\text{C}$ targets and a breakup threshold of 1.5 MeV, presented in Figs. 9b and 10b yield ratios of approximately 3.5% and 2%, respectively, for similar energies with respect to the Coulomb barrier. When the fact that the ${}^6\text{Li} \rightarrow \alpha + d$ breakup cannot proceed via dipole excitation is taken into account, and that such excitations are included in our model calculations which were based on a “ ${}^7\text{Li}$ ” projectile, the agreement is rather good. Therefore, our model calculations are sufficiently realistic to draw reliable conclusions.

Our conclusion is that the total breakup cross section is very sensitive to both the breakup threshold energy and the target, i.e. the relative importance of Coulomb effects. This sensitivity is in addition to any differences due to nuclear structure effects, e.g. while the ${}^6\text{Li} \rightarrow \alpha + d$ breakup has no dipole component, the ${}^6\text{He} \rightarrow \alpha + 2n$ breakup has a very strong dipole contribution. Therefore, drawing general inferences as to the effect of breakup on other reaction channels, in particular elastic scattering and fusion, from data for a single weakly-bound nucleus and a limited range of targets could be misleading. This may be particularly so when results obtained for the stable weakly-bound nuclei, ${}^6\text{Li}$, ${}^7\text{Li}$ and ${}^9\text{Be}$, are used to infer the influence of breakup for the weakly-bound halo nuclei such as ${}^6\text{He}$ and ${}^{11}\text{Li}$. This is particularly striking when we compare the elastic scattering angular distributions for the different breakup thresholds and targets obtained from our model calculations. In Figs. 11–13 we plot the elastic scattering angular distributions at incident energies of 35 MeV, 15 MeV and 5.4 MeV for the ${}^{208}\text{Pb}$, ${}^{58}\text{Ni}$ and ${}^{12}\text{C}$ targets, respectively. These energies yield $E_{\text{c.m.}}/V_{\text{B}}$ values of approximately 1.15, 1.18 and 1.21, respectively, chosen as coupling effects are usually largest for incident energies around 10% to 20% above the Coulomb barrier.

It will be noted that the elastic scattering angular distributions for a breakup threshold of 1.0 MeV are clearly distinguishable from those for the higher thresholds, and that the angular range over which the main difference between the results of calculations with and without coupling is apparent moves away

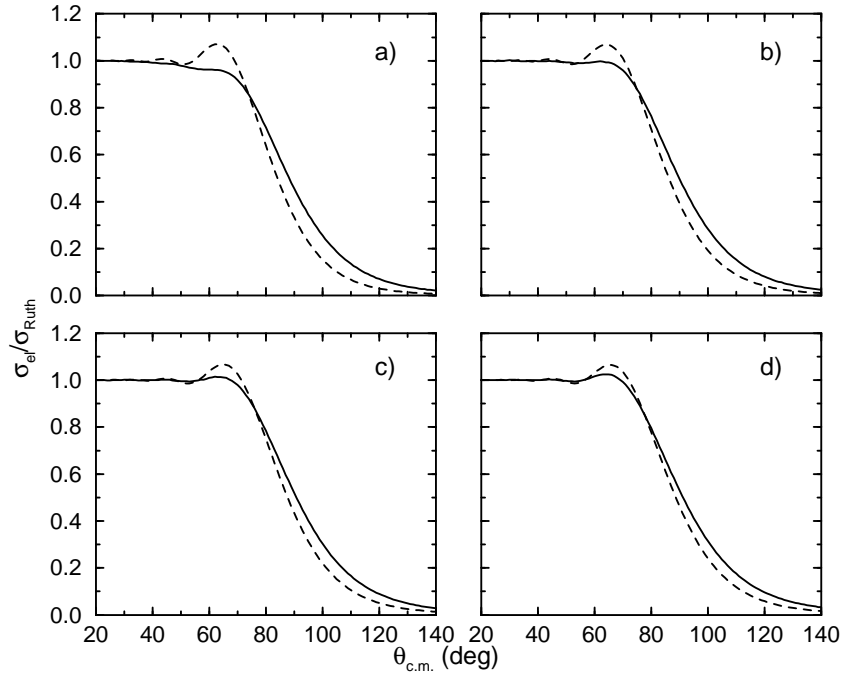


Figure 11: Model calculations for elastic scattering from a ^{208}Pb target at 35 MeV incident energy with breakup thresholds of a) 1.0 MeV, b) 1.5 MeV, c) 2.0 MeV and d) 2.5 MeV. The solid and dashed curves denote calculations with and without coupling to breakup, respectively.

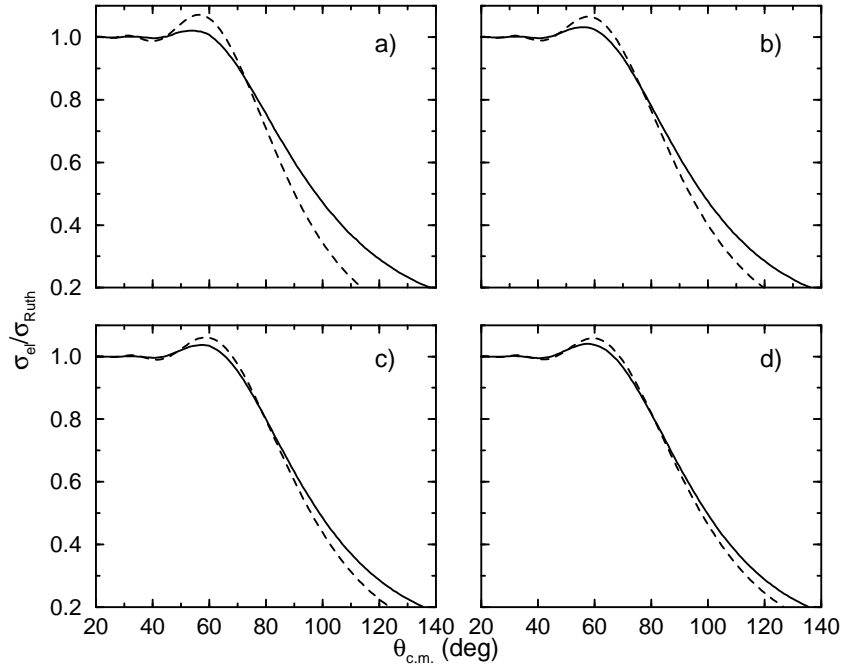


Figure 12: Model calculations for elastic scattering from a ^{58}Ni target at 15 MeV incident energy with breakup thresholds of a) 1.0 MeV, b) 1.5 MeV, c) 2.0 MeV and d) 2.5 MeV. The solid and dashed curves denote calculations with and without coupling to breakup, respectively.

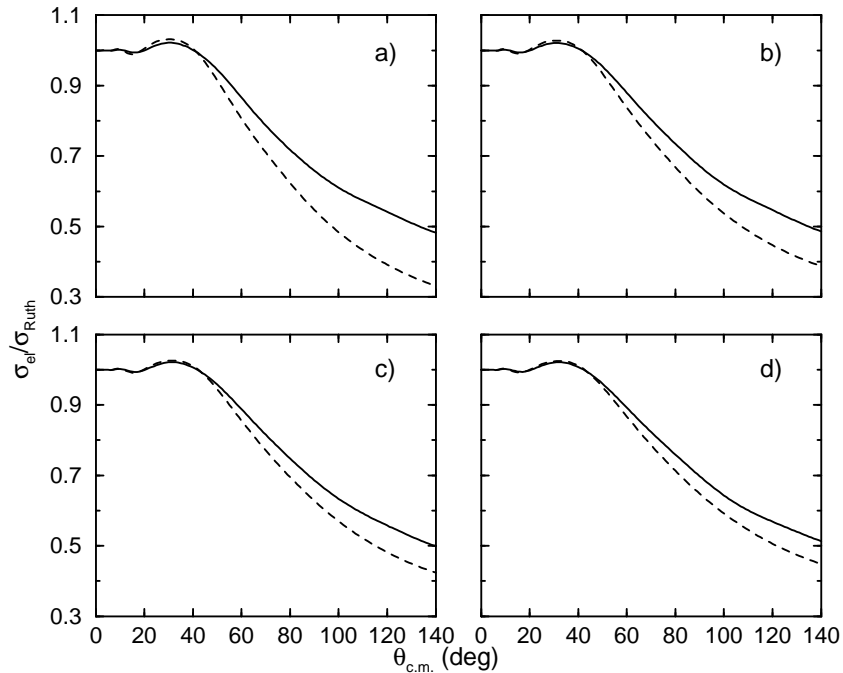


Figure 13: Model calculations for elastic scattering from a ^{12}C target at 5.4 MeV incident energy with breakup thresholds of a) 1.0 MeV, b) 1.5 MeV, c) 2.0 MeV and d) 2.5 MeV. The solid and dashed curves denote calculations with and without coupling to breakup, respectively.

from the Coulomb rainbow region to backward angles in passing from the ^{208}Pb to the ^{12}C target. The breakup coupling effect is also energy dependent; for the ^{12}C target at an incident energy of 12 MeV the angular distributions for the different breakup thresholds are indistinguishable. For a breakup threshold of 1.0 MeV the effect is much more dramatic for the ^{208}Pb target, at least in the angular region of the Coulomb rainbow, due to the effect of Coulomb breakup. This is in contrast to higher breakup thresholds where the influence of Coulomb breakup couplings on the elastic scattering has been found to be small, even for incident energies close to the Coulomb barrier, despite its importance for the total breakup cross section [130].

We thus see that breakup is a complex process, and that each system needs to be investigated on its own merits if we are to draw reliable conclusions concerning its influence on other reaction channels. This is particularly so in the case of halo nuclei, as their very low breakup thresholds lead to much stronger effects. However, even for halo nuclei, breakup is not an important contributor to the total reaction cross section except for systems where the Coulomb interaction dominates and then only for incident energies close to or below the top of the Coulomb barrier. It is therefore possible that the apparent contradictions as to whether sub-barrier fusion enhancement has been observed or not in different systems involving weakly-bound nuclei may be partly due to this “system dependence” — a system involving fusion with a lighter target may still exhibit an enhancement, but the effect may be too small to be observed. However, as we shall see in the next section, there are other system dependent effects that may be stronger than those due to breakup which further complicate the matter.

4.4 *Transfer reactions and their effect on other reaction channels*

As stated in section 4.1, in contrast to breakup, we have a reliable means of calculating the influence of transfer reactions on the fusion cross section through CRC calculations employing the ingoing-wave boundary condition or its equivalent. In this section we present such calculations for

$^{208}\text{Pb}(^6\text{He}, ^5\text{He})^{209}\text{Pb}$, $^{208}\text{Pb}(^8\text{He}, ^7\text{He})^{209}\text{Pb}$, $^{208}\text{Pb}(^6\text{Li}, ^5\text{Li})^{209}\text{Pb}$ and $^{60}\text{Ni}(^6\text{Li}, ^5\text{Li})^{61}\text{Ni}$ as representative examples. All calculations were carried out using the code FRESKO [107]. That transfer couplings can have significant effects on the elastic scattering for weakly bound nuclei was shown in the case of the $^9\text{Be} + ^{208}\text{Pb}$ system [109]. It was found that couplings to the positive Q -value $^{208}\text{Pb}(^9\text{Be}, ^8\text{Be})^{209}\text{Pb}$ transfer reaction produced a DPP with the same characteristics in the surface region as that produced by breakup, leading to a reduction in the real part of the effective potential and thus an increase in the effective Coulomb barrier. Thus, couplings to transfer reactions may be responsible for part of the reduction in the double folding model potentials found necessary for weakly bound nuclei referred to in section 4.3, and it is reasonable to suppose that they may also have important effects on fusion induced by such nuclei.

4.4.1 Conditions for the transfer calculations

We adopted a similar method to that used in [101], whereby our “bare” potentials in all channels consisted of a double-folded real part and an interior Woods-Saxon imaginary part to simulate the ingoing-wave boundary condition [103]. We used the M3Y effective interaction in the form of [119] and took the parameterisations of [131] for the ^6He and ^8He matter densities, the ^6Li matter density being taken from [132]. For the ^5He and ^7He matter densities we took the same form as [131], adjusting the parameters of the neutron part to give matter radii of 1.85 fm and 2.65 fm, respectively, close to the calculated values of [133] and [134]. We assumed the mirror hypothesis for ^5Li , taking the proton density as equal to the ^5He neutron density and *vice versa*, as sufficiently realistic for our purposes. The ^{208}Pb matter density was derived from the charge density of [135], unfolding the finite charge distributions of the proton and neutron as in [119] and assuming that $\rho_n = (N/Z)\rho_p$. The ^{209}Pb density was taken to be the same as that for ^{208}Pb . The ^{60}Ni matter density was taken from [136], the ^{61}Ni density being taken to be equal to that for ^{60}Ni . The Woods-Saxon imaginary potentials had parameters: $W = 50$ MeV, $R_W = 1.0 \times (A_p^{1/3} + A_t^{1/3})$ fm, $a_W = 0.3$ fm. The double-folded potentials were calculated with the code DFPOOT [137].

Couplings for single neutron transfer to the 0.0 MeV $9/2^+$, 1.57 MeV $5/2^+$, 2.03 MeV $1/2^+$, 2.49 MeV $7/2^+$ and 2.54 MeV $3/2^+$ states of ^{209}Pb were included in the $^{208}\text{Pb}(^6\text{He}, ^5\text{He})$, $^{208}\text{Pb}(^8\text{He}, ^7\text{He})$ and $^{208}\text{Pb}(^6\text{Li}, ^5\text{Li})$ calculations. The $n + ^{208}\text{Pb}$ binding potentials and spectroscopic factors were taken from the adiabatic model $^{208}\text{Pb}(d,p)$ analysis of [138]. The $n + ^5\text{He}$, $n + ^7\text{He}$ and $n + ^5\text{Li}$ binding potentials were of Woods-Saxon form, with $R_0 = 1.25 \times A^{1/3}$ fm, $a = 0.65$ fm and a spin-orbit term with the same geometry and a depth of 6 MeV, the depth of the central part being adjusted to obtain the correct binding energy. The $n + ^5\text{He}$, $n + ^7\text{He}$ and $n + ^5\text{Li}$ spectroscopic factors were taken from [139], [140] and [141], respectively. Stripping to the 1.27 MeV and 1.49 MeV $1/2^-$ states of ^5He and ^5Li , respectively, was included in addition to that to the $3/2^-$ ground state resonances. For the $^{60}\text{Ni}(^6\text{Li}, ^5\text{Li})$ calculations transfers to the 0.0 MeV $3/2^-$, 0.067 MeV $5/2^-$, 0.283 MeV $1/2^-$, 0.909 MeV $5/2^-$, 1.132 MeV $5/2^-$, 1.185 MeV $3/2^-$, 2.122 MeV $9/2^+$, 2.123 MeV $1/2^-$ and 3.482 MeV $9/2^+$ states of ^{61}Ni were included, the $n + ^{60}\text{Ni}$ binding potentials and spectroscopic factors being taken from [142].

4.4.2 Validity of transfer calculations: comparison to experimental data

Calculated excitation functions for the total one neutron transfer reaction, “bare” (i.e. no coupling) and CRC fusion cross sections are presented in Figs. 14–17 as functions of $E_{c.m.}/V_B$. The Coulomb barriers were calculated as the maxima of the combined “bare” nuclear plus Coulomb potentials in the respective entrance channels. We also plot data for the complete fusion of ^6He [24] and ^6Li [44] with ^{209}Bi and the total α production cross sections for the $^6\text{He} + ^{209}\text{Bi}$ [55] and $^6\text{Li} + ^{208}\text{Pb}$ [127] systems, plus the total $\alpha + p$ coincidence cross sections for $^6\text{Li} + ^{208}\text{Pb}$ [127]. The total fusion cross sections for ^6He and $^6\text{Li} + ^{209}\text{Bi}$ should be similar to those for a ^{208}Pb target. The total α production cross

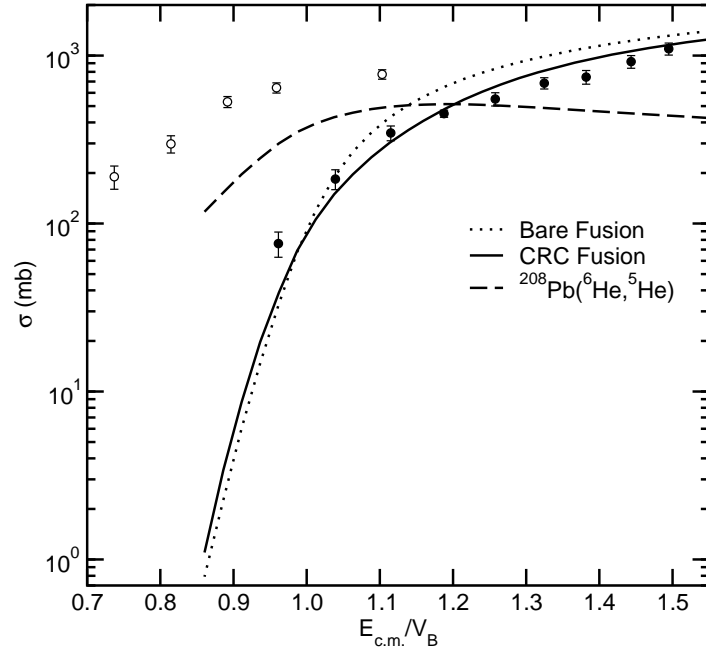


Figure 14: Calculated ${}^6\text{He} + {}^{208}\text{Pb}$ total fusion and ${}^{208}\text{Pb}({}^6\text{He}, {}^5\text{He}){}^{209}\text{Pb}$ excitation functions. The filled and open circles denote the total fusion and total α production cross sections for the ${}^6\text{He} + {}^{209}\text{Bi}$ system of [24] and [55], respectively.

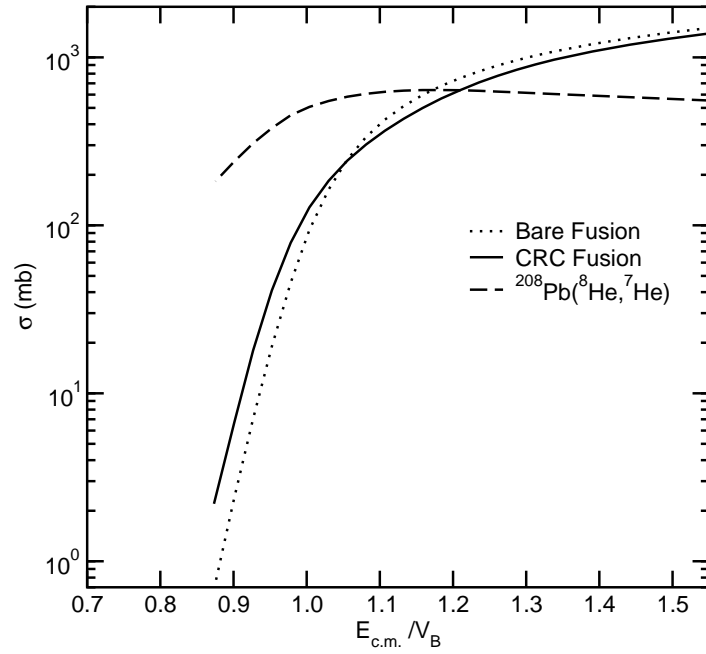


Figure 15: Calculated ${}^8\text{He} + {}^{208}\text{Pb}$ total fusion and ${}^{208}\text{Pb}({}^8\text{He}, {}^7\text{He}){}^{209}\text{Pb}$ excitation functions.

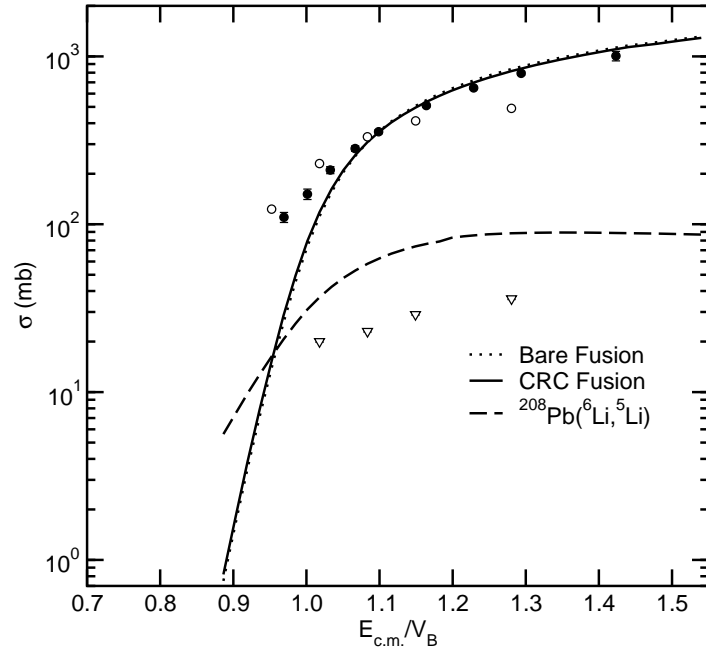


Figure 16: Calculated ${}^6\text{Li} + {}^{208}\text{Pb}$ total fusion and ${}^{208}\text{Pb}({}^6\text{Li}, {}^5\text{Li}){}^{209}\text{Pb}$ excitation functions. The filled circles denote the total fusion cross sections for the ${}^6\text{Li} + {}^{209}\text{Bi}$ system [44], while the open circles and triangles denote the total α production and total $\alpha + p$ coincidence cross sections, respectively, for the ${}^6\text{Li} + {}^{208}\text{Pb}$ system [127].

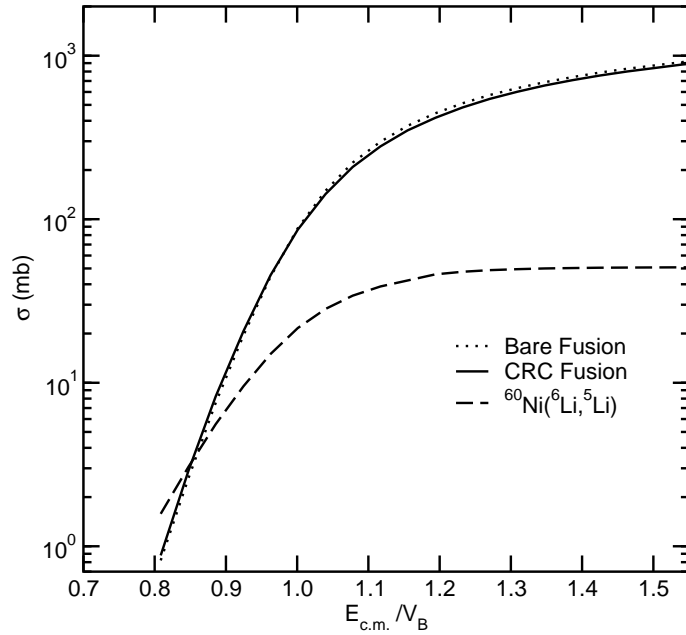


Figure 17: Calculated ${}^6\text{Li} + {}^{60}\text{Ni}$ total fusion and ${}^{60}\text{Ni}({}^6\text{Li}, {}^5\text{Li}){}^{61}\text{Ni}$ excitation functions.

section for ${}^6\text{He} + {}^{209}\text{Bi}$ should provide a reasonable estimate of that for a ${}^{208}\text{Pb}$ target, although nuclear structure differences may be more important here. We have chosen ${}^{208}\text{Pb}$ in preference to ${}^{209}\text{Bi}$ in order to have tractable calculations.

Before considering the effect on fusion of these couplings we shall compare the calculated transfer cross sections with existing measurements. For the ${}^6\text{He} + {}^{209}\text{Bi}$ system, $n + \alpha$ coincidence measurements indicate a total one neutron transfer cross section of (155 ± 25) mb at an incident energy of 22.9 MeV [57, 58], accounting for $(20 \pm 2)\%$ of the total α production cross section. Our calculated value at this energy is 510 mb, about three times larger. It is possible that part of the discrepancy is due to nuclear structure differences between ${}^{208}\text{Pb}$ and ${}^{209}\text{Bi}$ — ${}^{208}\text{Pb}$ is a very good core for a single-particle description of the ${}^{209}\text{Pb}$ nucleus, thus making calculation of the transfer much easier — but it is most likely due to the effect of other couplings not included in the calculations, such as breakup or two neutron transfer. Unfortunately, a meaningful calculation for the latter process is not possible, even for a ${}^{208}\text{Pb}$ target, due to lack of knowledge of the structure of the excited states of ${}^{210}\text{Pb}$ in the most important excitation energy region — even spins and parities are unknown. The situation is much worse for ${}^{211}\text{Bi}$ if one contemplated a similar calculation for a ${}^{209}\text{Bi}$ target, as not only are the spins and parities of the relevant states unknown, their number is considerably greater than in ${}^{210}\text{Pb}$. The cross section for two neutron transfer is found to be much larger than that for single neutron transfer in the ${}^6\text{He} + {}^{209}\text{Bi}$ system, approximately (400 ± 100) mb at angles greater than or equal to that of the “grazing peak”, or $(55 \pm 12)\%$ of the total α production cross section [58]. Thus it is possible that two-step transfer via the $({}^6\text{He}, {}^5\text{He})$, $({}^5\text{He}, {}^4\text{He})$ process may reduce the one neutron transfer cross section, although it is unlikely to account for the whole of the discrepancy. We note that test calculations using a ${}^5\text{He} + {}^{209}\text{Pb}$ double-folding potential calculated using a ${}^5\text{He}$ density with a larger r.m.s. matter radius did lead to a slight reduction in the calculated one neutron transfer cross section, although only of the order of a few percent. However, tests also found that including surface absorption, i.e. increasing the radius and diffuseness parameters of the imaginary potentials to more conventional values, considerably reduced the calculated transfer cross sections to better match the measured value. As increased surface absorption may be considered to simulate the effect of couplings to other channels not explicitly included, particularly the two neutron transfer which should contribute a strong surface absorption due to its large cross section, we conclude that the present calculations are adequate to investigate the effect of a single process, i.e. the $({}^6\text{He}, {}^5\text{He})$ single neutron transfer on the total fusion cross section.

Our calculated ${}^{208}\text{Pb}({}^6\text{Li}, {}^5\text{Li}){}^{209}\text{Pb}$ cross sections are approximately a factor of 2.5 greater than the measured total $\alpha + p$ cross sections of [127] and account for about 18% of the measured total α production cross section [127]. Single neutron transfer was not considered as a possible production mechanism for the observed $\alpha + p$ coincidences in [127], although it was discussed in an earlier article by the same group [69]. However, $\alpha + p$ coincidences in the ${}^6\text{Li} + {}^{208}\text{Pb}$ system have been previously observed in this energy range [143] and the projected spectrum shown in Fig. 18 clearly shows that this is indeed a transfer process populating known bound states in ${}^{209}\text{Pb}$. The reaction was found to proceed mainly via the ground state of ${}^5\text{Li}$ [143] and our calculations are consistent with this, the total transfer cross section with ${}^5\text{Li}$ in its ground state is approximately a factor of 9 greater than that with ${}^5\text{Li}$ in its first excited state at a ${}^6\text{Li}$ incident energy of 30 MeV. Similar remarks concerning the effect of increased surface absorption also apply here.

More refined calculations intended to model the direct reaction processes as accurately as possible are able to provide a good description of the available elastic scattering and $\alpha + d$ and $\alpha + p$ coincidence data for the ${}^6\text{Li} + {}^{208}\text{Pb}$ system. The ${}^6\text{Li} \rightarrow \alpha + d$ breakup was included using the CDCC technique as in [72] and the ${}^{208}\text{Pb}({}^6\text{Li}, {}^5\text{Li}){}^{209}\text{Pb}$ transfer was included as described above, with the exception that the ${}^5\text{Li} + {}^{209}\text{Pb}$ potential was calculated using the global ${}^6\text{Li}$ parameters of [144] — tests found that the results are not very sensitive to the choice of exit channel potential. Results are compared with the data of [127] in Fig. 19. Agreement between calculations and data is good (we have added error bars of 20% to the data, indicated in [127] as being the absolute accuracy of the exclusive data) with the

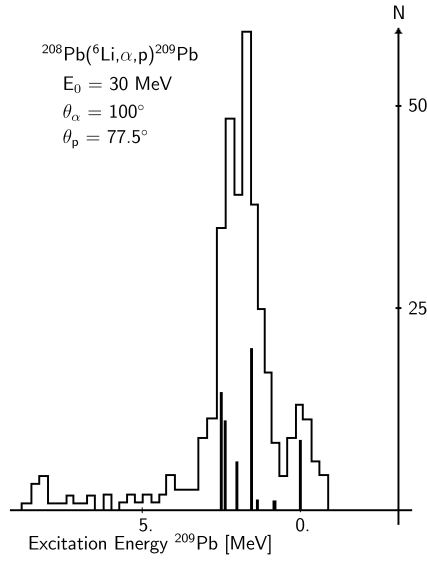


Figure 18: Projected $^{208}\text{Pb}(^6\text{Li}, \alpha, p)^{209}\text{Pb}$ spectrum adapted from [143]. The vertical bars indicate the total cross sections for the $^{208}\text{Pb}(d, p)^{209}\text{Pb}$ reaction.

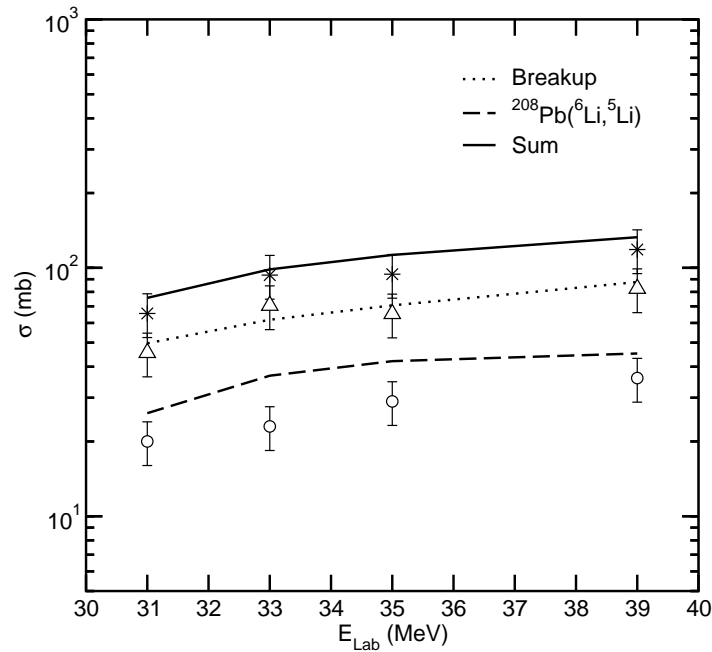


Figure 19: Results of more refined calculations of breakup and transfer for the $^6\text{Li} + ^{208}\text{Pb}$ system. The data are taken from [127] and represent the $\alpha + p$ coincidences (circles), $\alpha + d$ coincidences (triangles) and their sum (stars). The $\alpha + p$ coincidences are modelled as a $^{208}\text{Pb}(^6\text{Li}, ^5\text{Li})^{209}\text{Pb}$ transfer process.

Table 1: Reaction Q -values for the transfers considered in this section.

Reaction	Q -value
$^{208}\text{Pb}(^6\text{He}, ^5\text{He})^{209}\text{Pb}$	+2.07 MeV
$^{208}\text{Pb}(^8\text{He}, ^7\text{He})^{209}\text{Pb}$	+1.35 MeV
$^{208}\text{Pb}(^6\text{Li}, ^5\text{Li})^{209}\text{Pb}$	-1.73 MeV
$^{60}\text{Ni}(^6\text{Li}, ^5\text{Li})^{61}\text{Ni}$	+2.16 MeV

total calculated $^{208}\text{Pb}(^6\text{Li}, ^5\text{Li})^{209}\text{Pb}$ cross sections approximately 20% larger than the $\alpha + p$ coincidence data, a discrepancy easily accounted for by uncertainties in the $^6\text{Li} \rightarrow ^5\text{Li} + n$ form factor.

4.4.3 Results of calculations: effect of the couplings on fusion

Turning now to the effect of the transfer couplings on the calculated total fusion cross sections, we immediately see from Figs. 14-17 that qualitatively all the systems studied show the same behaviour, i.e. reduction above the barrier changing to enhancement below it. However, quantitatively, the two halo nuclei give very different results to those for ^6Li . Whereas the coupling effects are significant for ^6He and ^8He , both above and below the barrier, they are completely negligible for ^6Li for both targets. This is not simply a Q -value effect, as Table 1 shows — ^{60}Ni was deliberately chosen to give a $(^6\text{Li}, ^5\text{Li})$ Q -value close to that for $^{208}\text{Pb}(^6\text{He}, ^5\text{He})^{209}\text{Pb}$ — although this does play a rôle. The largest effect is due to the magnitude of the spectroscopic amplitudes (essentially $\sqrt{C^2S}$) — those for the $^6\text{He}/^5\text{He}$ overlap being approximately twice those for $^6\text{Li}/^5\text{Li}$ and that for $^8\text{He}/^7\text{He}$ nearly three times as large. Test calculations for $^{208}\text{Pb}(^6\text{Li}, ^5\text{Li})^{209}\text{Pb}$ with the $^6\text{Li}/^5\text{Li}$ spectroscopic amplitudes doubled showed a considerable increase in the effect on the calculated fusion cross section, in both the increase for sub-barrier energies and the decrease above the barrier.

The observation of this effect, i.e. sub-barrier enhancement and above-barrier reduction of the fusion cross section for coupling to reaction channels with positive Q -values, is not new, as the schematic two-channel calculations of [102] and [101] yield similar results, although the more sophisticated calculations of [101] yield a much smaller above barrier reduction of the fusion cross section for a positive Q -value when the couplings are treated as transfers rather than inelastic excitations. We also note that similar coupling effects on the calculated fusion cross section to those seen here were observed in an extensive analysis of the $^{18}\text{O} + ^{60}\text{Ni}$ system [82].

A comparison of the calculated total fusion cross sections with the measured values for the $^6\text{He} + ^{209}\text{Bi}$ and $^6\text{Li} + ^{209}\text{Bi}$ systems in Figs. 14 and 16 shows that at energies above the barrier our calculations provide a rather good description of the data. However, there is an important difference between the two systems in that the effect of the $^{208}\text{Pb}(^6\text{He}, ^5\text{He})^{209}\text{Pb}$ transfer couplings is essential to the good agreement between calculations and data, whereas for the $^6\text{Li} + ^{209}\text{Bi}$ system the single neutron transfer couplings have a negligible effect. At sub-barrier energies the $^6\text{Li} + ^{209}\text{Bi}$ system shows a clear enhancement of the total fusion cross section with respect to both the “bare” no coupling and the CRC calculations, while for the $^6\text{He} + ^{209}\text{Bi}$ system an enhancement is only seen at the lowest measured energy. For the $^6\text{Li} + ^{209}\text{Bi}$ system the transfer couplings have a negligible effect while for the $^6\text{He} + ^{209}\text{Bi}$ system the effect is too small to give good agreement with the lowest energy data point. Thus, we see that there are evidently other important couplings that must be included in the $^6\text{Li} + ^{209}\text{Bi}$ system, and possibly in the $^6\text{He} + ^{209}\text{Bi}$ system, if we are to obtain a good description of the total fusion excitation function over the whole energy range. These couplings could be breakup, target inelastic excitations or other transfer reactions, particularly the $(^6\text{He}, ^4\text{He})$ two-neutron transfer for the

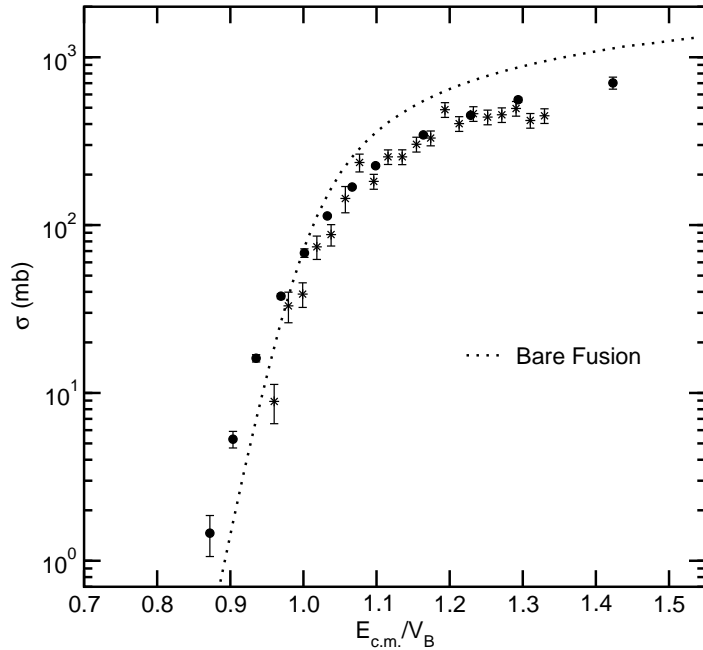


Figure 20: Calculated “bare” ${}^6\text{Li} + {}^{208}\text{Pb}$ fusion compared to measured ${}^6\text{Li} + {}^{209}\text{Bi}$ [44] (filled circles) and ${}^6\text{Li} + {}^{208}\text{Pb}$ [145] (stars) *complete* fusion excitation functions.

${}^6\text{He} + {}^{209}\text{Bi}$ system.

We finally consider the effects of couplings on the *complete* fusion cross section. In Fig. 20 we compare the bare fusion calculation for ${}^6\text{Li} + {}^{208}\text{Pb}$ to data for complete fusion in the ${}^6\text{Li} + {}^{209}\text{Bi}$ [44] and ${}^6\text{Li} + {}^{208}\text{Pb}$ [145] systems. The data for the two systems agree well for energies above the Coulomb barrier while at sub-barrier energies the ${}^6\text{Li} + {}^{208}\text{Pb}$ cross section falls more rapidly with energy. It is evident that a substantial fusion suppression is needed at above barrier energies in order to match either data set, while at sub-barrier energies the ${}^6\text{Li} + {}^{209}\text{Bi}$ data exhibit enhancement whereas the ${}^6\text{Li} + {}^{208}\text{Pb}$ data show a slight suppression. If this is a real effect it is probably not due to breakup, as the target is essentially a spectator in the breakup process and the extra unit of charge on the ${}^{209}\text{Bi}$ target would not be expected to be important.

To summarise, we find that transfer couplings, although rather neglected in the debate concerning the possible enhancement of fusion for halo nuclei, can have important effects. We also note that these effects are not limited to the sub-barrier region but are also important at energies above the barrier. In this respect our conclusions are similar to those of a detailed study of the ${}^{18}\text{O} + {}^{60}\text{Ni}$ system [82]. It is again evident that attempting to draw conclusions concerning halo nuclei from studies of the stable weakly-bound nuclei could be misleading.

5 Discussion

We have seen in the previous section that, in contrast to the stable weakly-bound nucleus ${}^6\text{Li}$, couplings to single neutron transfer reactions have an important influence on fusion induced by the neutron halo nuclei ${}^6\text{He}$ and ${}^8\text{He}$. This influence is manifest as an above-barrier reduction and a sub-barrier enhancement of the calculated fusion cross section relative to the no-coupling case, the above-barrier reduction being much more important than the sub-barrier enhancement for ${}^6\text{He}$, less so for ${}^8\text{He}$. While similar couplings produce a qualitatively similar effect for ${}^6\text{Li}$, it is entirely negligible. In this section we shall attempt to establish whether this is a universal phenomenon for halo nuclei. We will only

briefly discuss the complex and sometimes controversial question of the effect on fusion of coupling to breakup, due to the lack of a completely adequate model. The conclusions of the original analyses of the fusion data for weakly bound exotic nuclei presented in section 3.3 fall into two groups, those that infer a sub-barrier enhancement of the fusion cross section: ${}^6\text{He} + {}^{206}\text{Pb}$ [50] and ${}^6\text{He} + {}^{209}\text{Bi}$ [24], and those that infer no enhancement: ${}^6\text{He} + {}^{64}\text{Zn}$ [19], ${}^6\text{He} + {}^{238}\text{U}$ [18], ${}^7\text{Be} + {}^{238}\text{U}$ [65] and ${}^{11}\text{Be} + {}^{209}\text{Bi}$ [146]. However, enhancement (or lack of it) is inferred with respect to different references and different methods of “reducing” the data are adopted in the individual articles. In this section we shall also investigate whether a consistent analysis method can fit the ensemble of these data into a single, coherent picture.

5.1 Comparison between experimental data and calculations: conditions

In order to motivate the discussion, we compare the data for fusion induced by weakly bound radioactive nuclei on various targets already presented in section 3.3 with one-dimensional barrier penetration model calculations employing double-folded potentials. We also present similar calculations for fusion induced by the core nuclei interacting with the same targets, where available, for comparison purposes. The calculations are similar to those already described in section 4.4; we employ the same standard M3Y interaction with the ${}^6\text{He}$ matter density taken from [131], the ${}^7\text{Be}$ matter density from [147], the ${}^{10}\text{Be}$ and ${}^{11}\text{Be}$ matter densities from [148] and the ${}^4\text{He}$ matter density derived from the three parameter Fermi distribution charge density of [149] by unfolding the proton and neutron charge distributions as in [119] and assuming that $\rho_n = (N/Z)\rho_p$. Target matter densities were derived from charge densities in a similar way to that for ${}^4\text{He}$, the references being as follows: ${}^{64}\text{Zn}$ [150], ${}^{209}\text{Bi}$ [135] and ${}^{238}\text{U}$ [151]. The proton density for ${}^{206}\text{Pb}$ was obtained by unfolding the finite neutron and proton charge distributions from the charge density of [135] while the neutron density was taken from [152].

As discussed previously, this method of comparison is not completely unambiguous, as the double-folded potentials depend on the choice of effective nucleon-nucleon interaction and matter densities used to calculate them. We have chosen a standard M3Y effective interaction with no density dependence for the sake of simplicity; at the relatively low energies considered here this should be adequate. Modern density-dependent versions of the M3Y, e.g. the CDM3Y6 [153], could be used if a more sophisticated interaction is desired. The procedure used for extracting the target matter densities from empirical charge densities, while relatively standard, may be questioned [119] for nuclei where $N \neq Z$, even approximately. The matter densities for the radioactive beam nuclei are of necessity taken from calculations, although for ${}^6\text{He}$ we used a matter density deduced [131] from interaction cross section measurements assuming harmonic oscillator forms and yielding results similar to relativistic mean field calculations.

To investigate the level of uncertainty in the calculated fusion excitation functions we present in Figs. 21 and 22 calculations for the ${}^6\text{He} + {}^{208}\text{Pb}$ and ${}^6\text{He} + {}^{206}\text{Pb}$ systems, respectively, where the effects of choosing different ${}^6\text{He}$ matter densities and ${}^{206}\text{Pb}$ neutron densities are tested. Fig. 21 compares three calculations for the ${}^6\text{He} + {}^{208}\text{Pb}$ system using different ${}^6\text{He}$ matter densities [131, 148, 154]. The excitation functions calculated with the ${}^6\text{He}$ densities of Sagawa [148] and Al-Khalili *et al.* [154] show shifts of $\sim +0.3$ MeV and ~ -0.3 MeV, respectively, with respect to that calculated with the density of Tanihata *et al.* [131], consistent with the differences in the calculated Coulomb barrier heights. In Fig. 22 we compare fusion excitation functions for the ${}^6\text{He} + {}^{206}\text{Pb}$ system calculated using two different ${}^{206}\text{Pb}$ neutron density distributions. Both calculations use ${}^{206}\text{Pb}$ proton density distributions derived by unfolding the finite nucleon charge distributions from the charge density of [135]. The dotted curve employs the neutron density distribution of [152] while the dashed curve assumes that $\rho_n = (N/Z)\rho_p$. Again, we see a shift of ~ 0.3 MeV between the two curves, commensurate with the shift in the calculated Coulomb barrier heights. We thus see that the overall level of uncertainty is a shift in energy of the order of 1 MeV in the calculated fusion excitation function. Calculations based

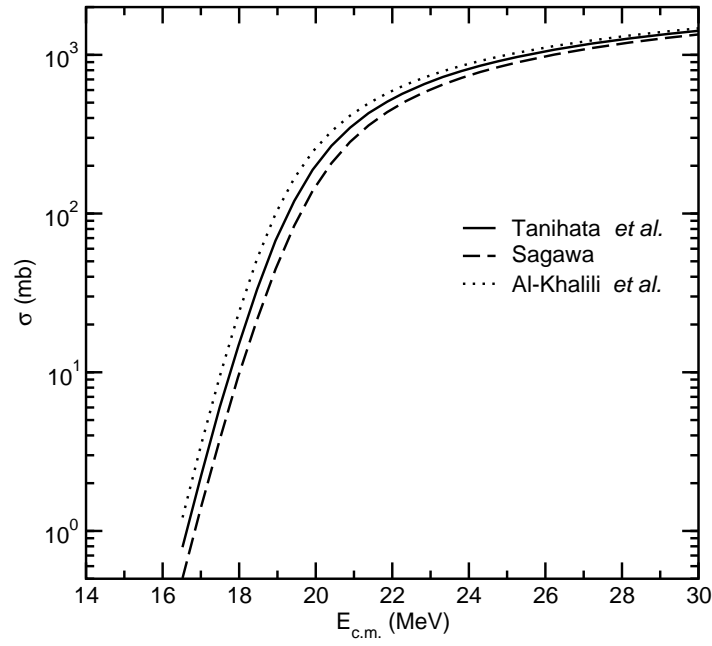


Figure 21: Calculated ${}^6\text{He} + {}^{208}\text{Pb}$ fusion excitation functions employing the densities of Tanihata *et al.* [131] (full curve), Sagawa [148] (dashed curve) and FC6 of Al-Khalili *et al.* [154] (dotted curve).

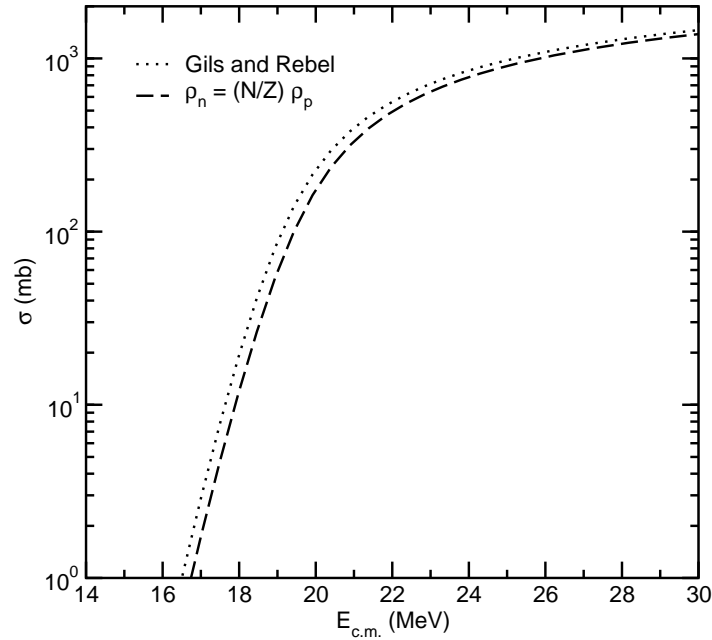


Figure 22: Calculated ${}^6\text{He} + {}^{206}\text{Pb}$ fusion excitation functions employing different neutron density distributions for ${}^{206}\text{Pb}$, from Gils and Rebel [152] (dotted curve) and derived from the proton distribution assuming that $\rho_n = (N/Z)\rho_p$ (dashed curve).

Table 2: Nominal Coulomb barrier heights for the systems considered in this section.

System	V_B
$^{64}\text{Zn} + ^4\text{He}$	9.50 MeV
$^{64}\text{Zn} + ^6\text{He}$	8.34 MeV
$^{206}\text{Pb} + ^6\text{He}$	19.04 MeV
$^{209}\text{Bi} + ^4\text{He}$	21.52 MeV
$^{209}\text{Bi} + ^6\text{He}$	19.44 MeV
$^{238}\text{U} + ^4\text{He}$	22.79 MeV
$^{238}\text{U} + ^6\text{He}$	20.76 MeV
$^{209}\text{Bi} + ^6\text{Li}$	29.97 MeV
$^{238}\text{U} + ^7\text{Be}$	43.43 MeV
$^{209}\text{Bi} + ^{10}\text{Be}$	39.30 MeV
$^{209}\text{Bi} + ^{11}\text{Be}$	37.12 MeV

on these double-folded potentials should therefore provide a reasonable basis for discussion, although the details of their comparison with experiment should be treated with due caution.

5.2 Results and discussion

We present in Figs. 23–28 fusion excitation functions calculated using the double-folded potentials obtained as described above and compare them with data for total fusion, with the exception of the $^6\text{He} + ^{64}\text{Zn}$ system where we plot both the “raw” residue cross sections of [19] which could contain events due to transfer reactions (referred to as “total fusion” for brevity) and the “corrected” cross section where the measured ^{65}Zn cross section has been replaced by that calculated with the code CASCADE [155] (referred to as “complete fusion” for brevity), the $^6\text{He} + ^{238}\text{U}$ [18] and $^7\text{Be} + ^{238}\text{U}$ [65] systems where we plot the *complete* fusion² and fission cross sections (the total fusion cross section should fall somewhere between the two), the $^4\text{He} + ^{238}\text{U}$ system where we plot the fission cross sections [18, 156, 157] (which should, however, essentially equate to the total fusion cross section) and the $^6\text{He} + ^{206}\text{Pb}$ system where we plot the $(^6\text{He}, 2n)$ cross sections of [50]. In the following discussion enhancement and suppression of fusion are defined relative to the “bare” fusion calculations denoted by the dotted curves in Figs. 23–28. The calculated nominal Coulomb barriers are given in Table 2.

We may draw some general conclusions from these figures, bearing in mind the caveats concerning the double-folded potentials. With the possible exception of the $^4\text{He} + ^{64}\text{Zn}$ system where the various data sets do not agree very well with each other, the data for total fusion of the “core” nuclei are rather well described for energies above the Coulomb barrier, taking into account a certain amount of scatter in the data points for some systems. Where data points exist for sub-barrier energies the enhancement of measured to calculated fusion cross sections characteristic of “normal” nuclei, see e.g. [4, 5, 85], is also observed for these systems, with the possible exception of $^4\text{He} + ^{238}\text{U}$ where the different data sets disagree at sub-barrier energies. The level of agreement obtained for the core fusion excitation functions at above barrier energies where we expect coupling effects to be small for these systems, at least for those with ^4He projectiles, suggests that our adopted effective nucleon-nucleon interaction and target

²Actually events leading to fission without a charged residue. See also the discussion in sections 3.3.4 and 3.3.5.

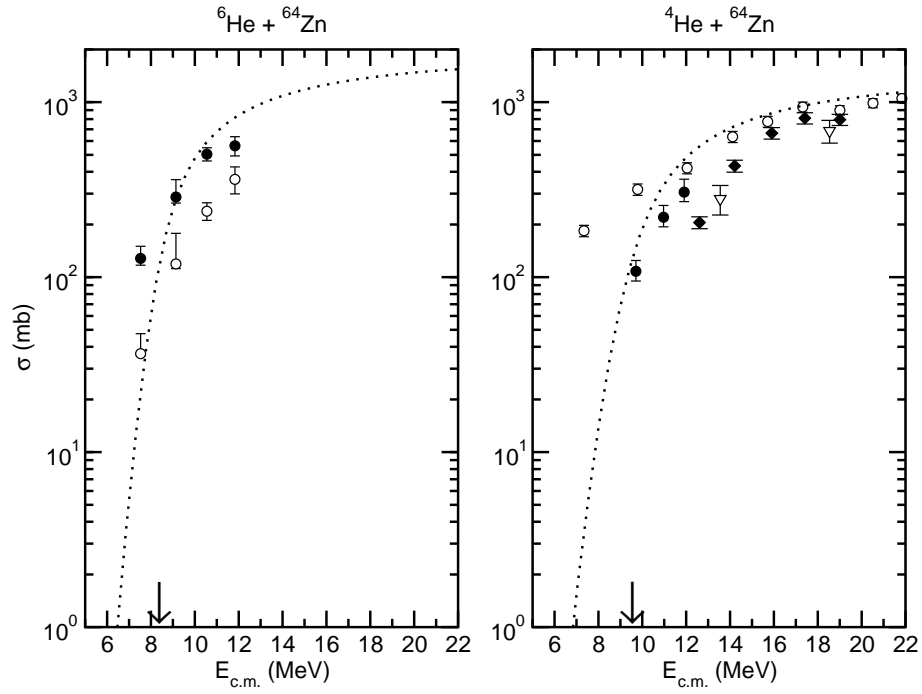


Figure 23: Calculated ${}^6\text{He} + {}^{64}\text{Zn}$ (left) and ${}^4\text{He} + {}^{64}\text{Zn}$ (right) fusion excitation functions compared with the total fusion data of Di Pietro *et al.* [19] (filled circles), the sum of the ${}^{64}\text{Zn}({}^4\text{He},n)$, ${}^{64}\text{Zn}({}^4\text{He},p)$, ${}^{64}\text{Zn}({}^4\text{He},2n)$, ${}^{64}\text{Zn}({}^4\text{He},np)$ and ${}^{64}\text{Zn}({}^4\text{He},n+{}^4\text{He})$ data of Levkovskiy [158] (open circles), and the sum of the ${}^{64}\text{Zn}({}^4\text{He},n)$ and ${}^{64}\text{Zn}({}^4\text{He},p)$ data of Ruddy and Pate [159] (open triangles) and Porile [160] (filled diamonds). The open circles on the left hand plot denote the corrected ${}^6\text{He} + {}^{64}\text{Zn}$ complete fusion data of Di Pietro *et al.* [19] corrected for the Coulomb barriers.

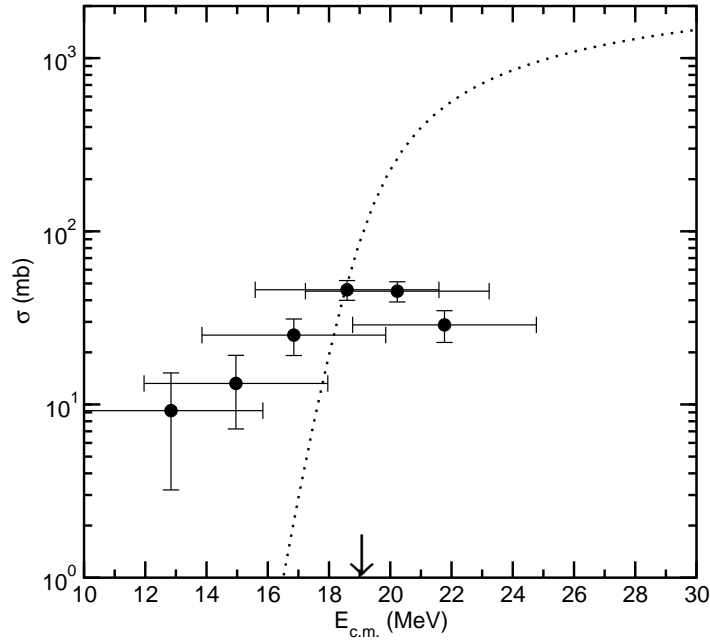


Figure 24: Calculated ${}^6\text{He} + {}^{206}\text{Pb}$ fusion excitation function compared with the ${}^{206}\text{Pb}({}^6\text{He},2n)$ data of Penionzhkevich *et al.* [50]. The arrow indicates the position of the calculated Coulomb barrier.

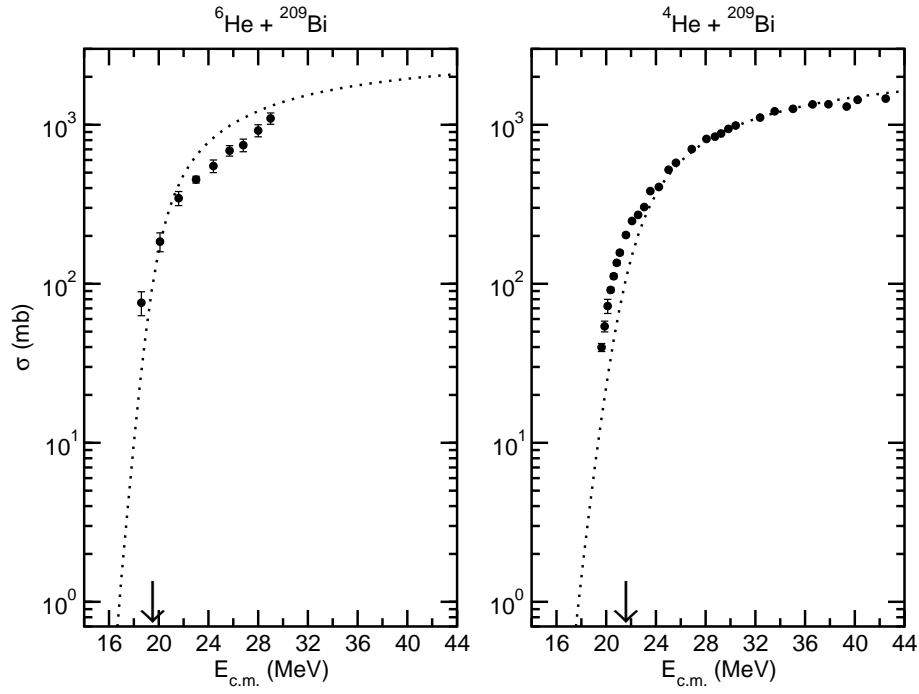


Figure 25: Calculated ${}^6\text{He} + {}^{209}\text{Bi}$ (left) and ${}^4\text{He} + {}^{209}\text{Bi}$ (right) fusion excitation functions compared with the total fusion data of Kolata *et al.* [24] and Barnett and Lilley [161] and Ramler *et al.* [162], respectively. The arrows indicate the positions of the calculated Coulomb barriers.

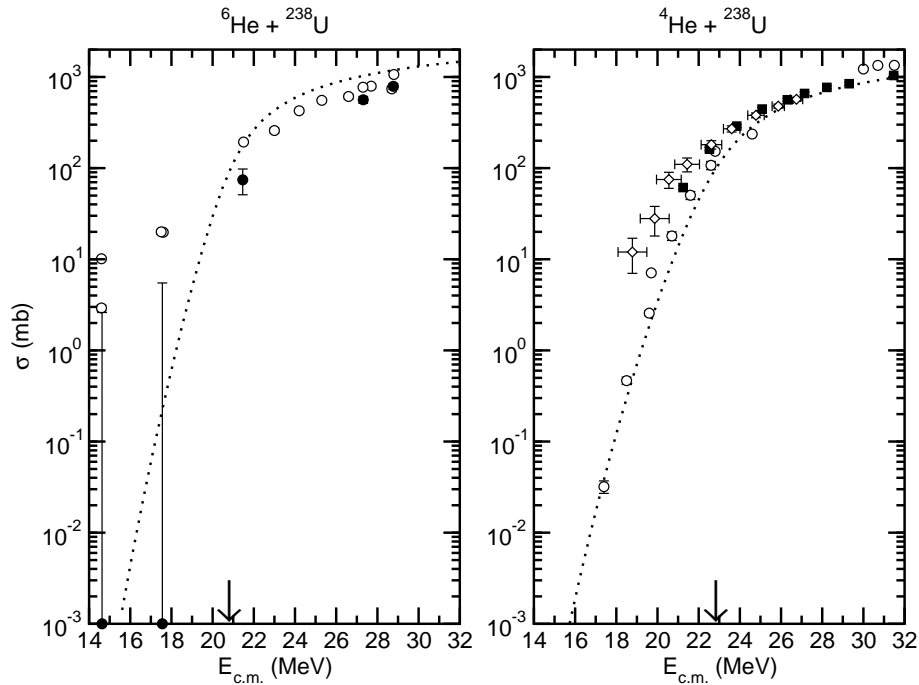


Figure 26: Calculated ${}^6\text{He} + {}^{238}\text{U}$ (left) and ${}^4\text{He} + {}^{238}\text{U}$ (right) fusion excitation functions compared with the *complete* fusion (filled circles) and fission (open circles) data of Raabe *et al.* [18]. The filled squares and open diamonds denote the fission data of Viola and Sikkeland [156] and Zaika *et al.* [157], respectively. The arrows indicate the positions of the calculated Coulomb barriers.

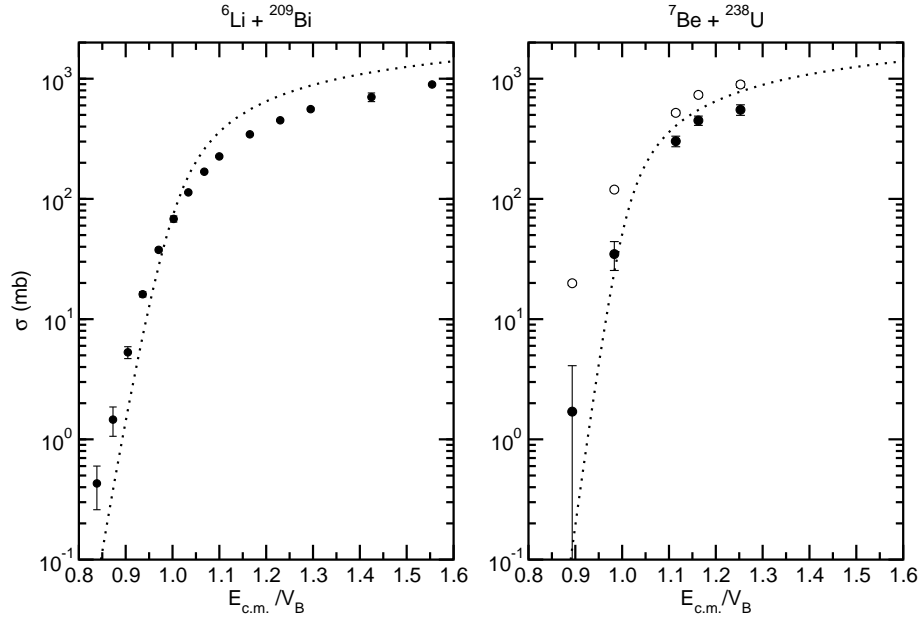


Figure 27: Calculated ${}^6\text{Li} + {}^{209}\text{Bi}$ (left) and ${}^7\text{Be} + {}^{238}\text{U}$ (right) fusion excitation functions compared with the *complete* fusion data of Dasgupta *et al.* [44] and Raabe *et al.* [65], respectively. The open circles denote the fission cross sections of Raabe *et al.* [65].

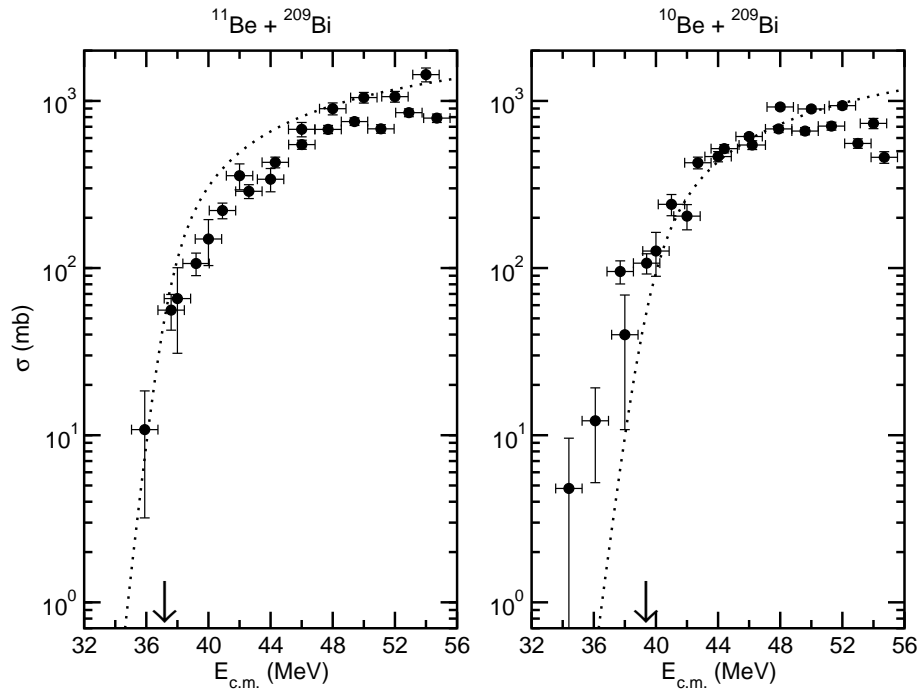


Figure 28: Calculated ${}^{11}\text{Be} + {}^{209}\text{Bi}$ (left) and ${}^{10}\text{Be} + {}^{209}\text{Bi}$ (right) fusion excitation functions compared with the total fusion data of Signorini *et al.* [146] and Signorini [163], respectively. The arrows indicate the positions of the calculated Coulomb barriers.

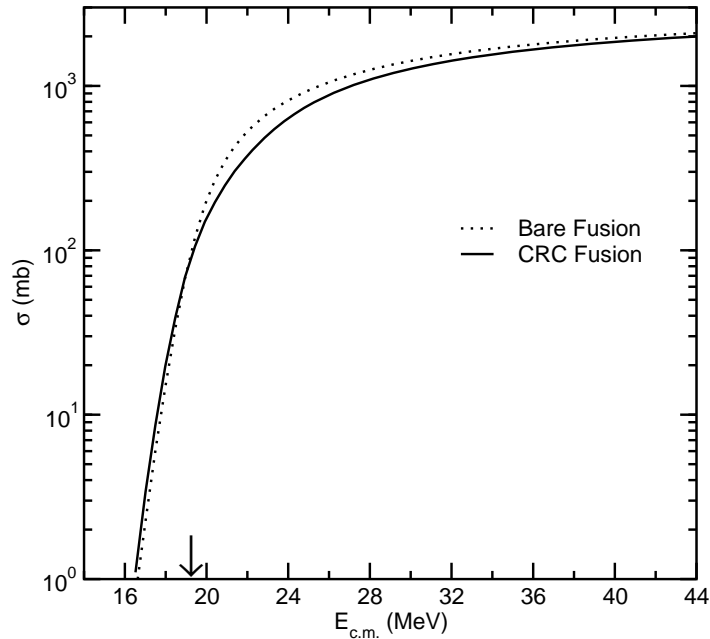


Figure 29: Calculated ${}^6\text{He} + {}^{208}\text{Pb}$ total fusion with (full curve) and without (dotted curve) coupling to the $({}^6\text{He}, {}^5\text{He})$ stripping. The arrow indicates the position of the calculated Coulomb barrier.

matter densities are physically reasonable.

The total fusion data for the halo nuclei are also consistent with a possible sub-barrier enhancement of total fusion, although this conclusion is very tentative, to say the least, as it rests solely on the lowest energy data points in the ${}^6\text{He} + {}^{64}\text{Zn}$, ${}^6\text{He} + {}^{206}\text{Pb}$ and ${}^6\text{He} + {}^{209}\text{Bi}$ systems. The other systems do not actually rule out the possibility of sub-barrier enhancement, either because the data stop short of the energies at which enhancement would be readily apparent or due to uncertainties in the data, due to the difficulty of defining unambiguously a fusion event at these low energies and/or poor statistics due to the low cross sections. Bearing in mind the uncertainties in the double-folded potentials discussed above and their effect on the calculated fusion excitation functions, sub-barrier enhancement of the total fusion cross section for halo nuclei remains to be confirmed.

The most striking general conclusion with regard to total fusion for the halo nuclei is not, however, concerned with the sub-barrier regime but rather with the suppression of the measured total fusion cross sections compared to the “bare” no-coupling calculations at energies a few MeV above the nominal Coulomb barriers. With the exception of the ${}^6\text{He} + {}^{206}\text{Pb}$ system where only ${}^{206}\text{Pb}({}^6\text{He}, 2n)$ data are available — essentially equivalent to total fusion for energies below the Coulomb barrier — and we consequently cannot comment on the above barrier fusion, all the total fusion excitation functions for the halo systems studied here exhibit this characteristic behaviour. This is particularly noticeable for the ${}^6\text{He} + {}^{209}\text{Bi}$, ${}^{238}\text{U}$ and ${}^{11}\text{Be} + {}^{209}\text{Bi}$ systems. This is in complete contrast to the total fusion excitation functions for the core nuclei, with the possible exception of the ${}^4\text{He} + {}^{64}\text{Zn}$ system. This suppression compared to the “bare” calculation for the halo nuclei is identical to that due to coupling to the single neutron stripping reaction in the CRC calculations presented in section 4.4 for the ${}^{6,8}\text{He} + {}^{208}\text{Pb}$ systems. There are hints in the data that the suppression factor peaks somewhat above the barrier and then diminishes as the bombarding energy is increased. In Fig. 29 we present calculations for the ${}^6\text{He} + {}^{208}\text{Pb}$ system showing the effect of coupling to the $({}^6\text{He}, {}^5\text{He})$ stripping over an extended energy range which exhibit this feature.

It is therefore tempting to conclude that single neutron stripping reactions are indeed responsible for this important suppression of the *total* fusion of neutron halo nuclei at energies just above the Coulomb

barrier. It should, however, be borne in mind that our calculations probe the effect of coupling to one reaction partition — single neutron stripping — in isolation. Other couplings, in particular two neutron transfer and breakup, may modify the overall effect. Nevertheless, the suggestion that this large effect due to neutron transfer is a general phenomenon and not just confined to the fusion of ${}^6\text{He}$ with heavy targets is borne out by test calculations which show similar effects due to the (${}^6\text{He}, {}^5\text{He}$) and (${}^{11}\text{Be}, {}^{10}\text{Be}$) couplings in the ${}^6\text{He} + {}^{58}\text{Ni}$ and ${}^{11}\text{Be} + {}^{208}\text{Pb}$ systems. However, while the transfer couplings do contribute to a sub-barrier enhancement of the total fusion they are far from being able to account for the whole of the effect seen in Fig. 24 for the ${}^6\text{He} + {}^{206}\text{Pb}$ system, for example. The important influence of transfer couplings on total fusion for halo nuclei at energies above the barrier is in complete contrast to the negligible effect these couplings have on fusion for the stable weakly bound nucleus ${}^6\text{Li}$, see section 4.4. However, it is similar to the effect of transfer couplings on fusion in the ${}^{18}\text{O} + {}^{58}\text{Ni}$ system [82], for example, although there the main above barrier suppression is due to two neutron transfer.

It is suggestive that fusion induced by ${}^{18}\text{O}$ exhibits the same important influence of transfer couplings on the above barrier fusion as we appear to see for the halo nuclei and that in both cases the transfer reactions have positive Q -values. However, as we have seen in section 4.4 a positive Q -value alone is not sufficient to obtain a significant effect from coupling to a transfer partition. In fact, the effect of a given set of couplings on other observables is a complex combination of Q -values, angular momentum matching conditions and spectroscopic factors, or more generally coupling strengths.

We note that the three-body time-dependent wave-packet model calculations of [104] show similar above barrier suppression of the total fusion cross section to that found in our CRC calculations. However, they see no sub-barrier enhancement; their results show either essentially no effect or a slight suppression in the sub-barrier energy regime.

A sub-barrier enhancement due to multiple neutron transfer is predicted in the Stelson model [59]: according to this picture, the weak binding of the neutrons in the projectile should favour the formation of a “neck” between the two reacting nuclei, thus helping to overcome the Coulomb barrier. We should however underline that this is a phenomenological model, ignoring the essential coupled-channel nature of the reaction mechanism.

We have so far not discussed the question of *complete* fusion involving halo nuclei and the effect of couplings thereon as with the exception of the ${}^6\text{He} + {}^{238}\text{U}$ and ${}^6\text{He} + {}^{206}\text{Pb}$ systems the available data are for total fusion. Clearly, the complete fusion cross sections will be rather smaller in magnitude than those for total fusion, although exactly how much smaller will depend on the system under consideration. Thus the suppression at above barrier energies should be somewhat larger for complete fusion than for total fusion and the sub-barrier enhancement (if present) smaller. The additional above barrier suppression for complete compared to total fusion could be considerable judging by the data for the ${}^6\text{Li} + {}^{209}\text{Bi}$ system, cf. Figs. 16 and 20, although as we have seen this may not be a reliable guide for the case of halo nuclei. Other couplings may well be needed to account for any extra suppression in the complete fusion and an obvious candidate is breakup. The calculations of [164, 165], for example, support this conjecture.

In Fig. 27 we compare the complete fusion cross sections for the ${}^6\text{Li} + {}^{209}\text{Bi}$ [44] and ${}^7\text{Be} + {}^{238}\text{U}$ [65] systems with the calculated bare fusion excitation functions. Although ${}^7\text{Be}$ is weakly bound it is not a halo nucleus, and is expected to exhibit behaviour similar to ${}^6\text{Li}$ due to its similar breakup threshold [166]. This does indeed appear to be the case as far as the complete fusion is concerned, as we see similar suppression at above barrier energies to that observed for ${}^6\text{Li}$. However, it is less marked and there is no evidence of a sub-barrier enhancement similar to that seen in the ${}^6\text{Li} + {}^{209}\text{Bi}$ system, although the uncertainties in the sub-barrier data points for ${}^7\text{Be} + {}^{238}\text{U}$ do not completely rule out this possibility. It is not possible to say whether the above-barrier *total* fusion is reasonably well described by the bare fusion calculation, as in the ${}^6\text{Li} + {}^{209}\text{Bi}$ case, although again the available data do not rule out this possibility (the total fusion cross section should lie somewhere between the complete fusion and

fission cross sections).

We shall now briefly discuss the question of the effect of coupling to breakup on fusion for halo nuclei. It is clear that any large sub-barrier enhancement of total fusion compared to a no-coupling calculation could not be accounted for by coupling to single neutron stripping, judging by the calculations for the ${}^6\text{He} + {}^{208}\text{Pb}$ system presented in Figs. 14 and 29. While couplings to inelastic excitation of the target should contribute to any sub-barrier enhancement of total fusion, the bulk of any effect may well be due to coupling to breakup and/or two neutron transfer, although for single neutron halo systems like ${}^{11}\text{Be}$ the latter process is not expected to be important. Most coupled channels based calculations suggest that the effect of coupling to breakup on the *total* fusion for sub-barrier energies should be an enhancement, although the extent of this enhancement and the bombarding energy at which it sets in depend on the details of the calculation, see e.g. [47] for a review of the literature on this subject. The extent of any enhancement may also depend quite sensitively on the breakup threshold energy, see e.g. [167]. We have already seen in section 4.3 that the magnitude of the breakup cross section and the effect of coupling to breakup on the elastic scattering angular distribution can be quite sensitive to the breakup threshold energy, depending on the target nucleus.

The situation for sub-barrier *complete* fusion is less clear. The ${}^{206}\text{Pb}({}^6\text{He},2n)$ data of [50] might be equated to complete fusion at sub-barrier energies with a reasonable degree of confidence, thus indicating a sub-barrier enhancement of the complete fusion cross section, although this is only really observed at the lowest energy measured due to the uncertainties in the incident energies. However, it is less certain whether coupling to breakup will also lead to a sub-barrier enhancement of complete fusion. Penionzhkevich *et al.* [50] accounted for sub-barrier enhancement in their ${}^{206}\text{Pb}({}^6\text{He},2n)$ data by a “sequential fusion” mechanism [52] with transfer of the two “valence” neutrons of ${}^6\text{He}$ followed by fusion of the ${}^4\text{He}$ core. However, the data for events leading to fission without a charged residue for the ${}^6\text{He} + {}^{238}\text{U}$ system (probably equivalent to complete fusion) are consistent with no sub-barrier enhancement, although the large uncertainties in the sub-barrier data points — it is clear that the cross section for these events is small compared to that for total fission — mean that the possibility of enhancement in this system cannot be entirely ruled out.

However, perhaps the most remarkable feature of reactions involving halo nuclei is not concerned with fusion at all, but rather direct reactions. Very large total reaction cross sections at near and sub-barrier energies have been observed in the ${}^6\text{He} + {}^{209}\text{Bi}$ [55] and ${}^6\text{He} + {}^{64}\text{Zn}$ [19] systems. These large cross sections have been identified with α production arising from direct reactions: ${}^6\text{He} \rightarrow \alpha + 2n$ breakup, $({}^6\text{He}, {}^5\text{He})$ transfer and $({}^6\text{He}, {}^4\text{He})$ transfer. Indeed, a total α production cross section of nearly 200 mb was observed for the ${}^6\text{He} + {}^{209}\text{Bi}$ system at an incident energy 6 MeV *below* the nominal Coulomb barrier [55]. For the ${}^6\text{He} + {}^{209}\text{Bi}$ system further exclusive measurements employing $\alpha + n$ coincidences have further established that the α production cross section is dominated by transfer; approximately 75% [57, 58] at an incident energy of ~ 23 MeV with $2n$ transfer contributing the largest share. The dominant contribution of transfer to the observed sub-barrier fission yield in the ${}^6\text{He} + {}^{238}\text{U}$ system [18] is consistent with this picture. Thus, for halo systems the total reaction cross section at sub-barrier energies seems to be dominated by the direct component, fusion giving a negligible contribution. While the direct reaction cross section is also observed to be larger than fusion at sub-barrier energies in other systems, see e.g. Fig. 16 for the ${}^6\text{Li} + {}^{209}\text{Bi}$ system and [168] for the ${}^{16,18}\text{O} + {}^{208}\text{Pb}$ and ${}^{15}\text{N}, {}^{16}\text{O} + {}^{209}\text{Bi}$ systems, it is the size of the effect for the halo systems that is remarkable; direct reactions completely dominate the total reaction cross section at these energies, unlike in other systems. Test calculations support the inference that this is a general phenomenon for halo systems; calculations of the ${}^{58}\text{Ni}({}^6\text{He}, {}^5\text{He}){}^{59}\text{Ni}$ and ${}^{208}\text{Pb}({}^{11}\text{Be}, {}^{10}\text{Be}){}^{209}\text{Pb}$ reactions exhibit a similar dominance over the calculated fusion at near and sub-barrier energies, as do calculations for the ${}^{208}\text{Pb}({}^8\text{He}, {}^7\text{He}){}^{209}\text{Pb}$ reaction, see Fig. 15.

In summary, a consistent analysis of the available data suggests that the total fusion excitation functions for neutron halo nuclei exhibit common behaviour so far as the limited sample of systems and

range of energies allows a general conclusion to be drawn. The data are consistent with an above barrier suppression and possibly a sub-barrier enhancement of the total fusion cross section, although the latter remains to be confirmed. While the above barrier suppression may be accounted for in large part by coupling to single neutron stripping, any sub-barrier enhancement is most probably due to coupling to two neutron transfer and/or breakup, depending on the system. However, much more remarkable are the very large near and sub-barrier direct reaction cross sections, dominating fusion by orders of magnitude. These also appear to be a general feature of reactions involving halo systems.

6 Conclusions

In this paper we have described the current experimental and theoretical situation concerning reactions with light unstable nuclei at energies around the Coulomb barrier. We saw on the one hand the problems related to the measurements, due to the quality of the available beams of light radioactive ions, and on the other hand the difficulties associated with trying to predict the behaviour of such systems theoretically. The latter are mainly connected with poor knowledge of the parameters involved in the description (details of nuclear structure, the positions and characteristics of excited states, spectroscopic factors, etc.) and, in the specific case of the coupling of breakup to fusion, to the lack of an adequate model.

Given the limited sample of systems for which data are currently available and the large uncertainties in some of the data sets — inevitable due to the difficulty of the experiments — it may seem premature to attempt to draw general conclusions concerning reactions involving halo nuclei. Nevertheless, in our investigations we came across some recurring features. Within the constraints imposed by the problems mentioned above, we may summarise these features as follows:

1. In general, the magnitude of a reaction channel is not a reliable indicator of the effect that, through coupling, that channel may have on elastic scattering or fusion. This was shown by calculations for the case of breakup and elastic scattering. For fusion, it goes back to the observation made in [10] that the transmitted flux (and thus fusion) and the reflected flux (the measured exit channels) are determined by different regions of the radial couplings.
2. Concerning fusion we observe the following: compared to “bare” no-coupling one-dimensional barrier penetration model calculations employing reasonably realistic double-folded potentials, the measured total fusion data for halo nuclei consistently show an above barrier suppression. There is some evidence that the degree of suppression peaks somewhat above the nominal Coulomb barrier then gradually declines as the incident energy is increased. The data for total fusion are also consistent with a possible sub-barrier enhancement, although this remains to be confirmed. Calculations suggest that the above barrier suppression may be attributed in large part to the effect of coupling to single neutron transfer reactions, although breakup will also contribute [98]. Any significant enhancement at sub-barrier energies must be due to other couplings, most probably breakup and/or two neutron transfer (depending on the system).
3. As the *complete* fusion cross section will be smaller than the total fusion we anticipate an increased above barrier suppression of complete fusion compared to total fusion and a smaller sub-barrier enhancement, if this is proved to be present. Depending on the system, couplings in addition to single neutron transfer may be needed to adequately describe the increased above barrier suppression.
4. Reactions involving halo nuclei exhibit a remarkable dominance of direct reactions over fusion at near and sub-barrier energies. The cross sections for direct reactions can be orders of magnitude larger than fusion at sub-barrier energies, a phenomenon that appears to be unique to halo systems.

The most important component of the direct reaction cross section is probably due to neutron transfers; this has been shown experimentally for the ${}^6\text{He} + {}^{209}\text{Bi}$ system and is borne out by calculations for other systems. Despite the relatively low thresholds, breakup does not seem to be a very large component of the total reaction cross section for the halo systems studied here, a conclusion that is again largely borne out by calculations.

These are our conclusions based on the currently available data for halo nuclei, but what of the future? Clearly, further data are highly desirable extending to other halo systems such as ${}^8\text{He}$, ${}^{11}\text{Li}$, ${}^{14}\text{Be}$, ${}^{15}\text{C}$ and others. Post-accelerated beams of some of these nuclei are already available, for example ${}^{11}\text{Li}$ at TRIUMF/ISAC in Canada. However, the current intensities (10^3 – 10^4 pps) are still too low to allow measurements of fusion at barrier energies. A significant increase in intensity will be brought about only by the next generation of radioactive beam facilities currently under construction or development. However, much can still be done in the way of improving our knowledge of nuclei for which beams of higher intensity (at least 10^5 pps) are already available. In particular, measurements of the total fusion for ${}^6\text{He}$ at far sub-barrier energies with good energy definition and reasonable statistics are needed to decide the question of sub-barrier fusion enhancement in a definitive manner. Extension of the available data to systems with lighter mass targets is also desirable, although the difficulty of defining a reliable signature for fusion in this mass range could be an obstacle [19, 20]. Further use could be made of available beams of ${}^8\text{He}$ — so far there is a single measurement of the elastic scattering of ${}^8\text{He}$ from a medium mass target [20] — which is expected to show an even larger sub-barrier reaction cross section than ${}^6\text{He}$, cf. Figs. 14 and 15.

Choice of target is also an important consideration from both the experimental and theoretical points of view. Experimentally, in measurements of fusion choice of target is often limited by considerations of a clear signature for fusion. It is unfortunate that most of the available data for fusion involving halo systems are thus for targets such that a comprehensive theoretical analysis including couplings to transfer reactions is not possible, due to the density of states and lack of the necessary nuclear structure information. While the experimental constraints are probably most severe, there should be scope for compromise choices where a reasonably complete calculation is possible without compromising the measurement. If the effect of coupling to two neutron transfer on fusion is to be elucidated, careful choice of the target will be required.

Further developments in the theory describing fusion of weakly bound nuclei in general are also required. In particular, more sophisticated treatments of the incomplete fusion process within a CDCC-type formalism are needed. The ideal would be to combine such methods with a CRC calculation of transfer, although we are still a considerable way from achieving this goal.

To counter the low beam intensities, the various experimental techniques used for the detection of fusion and direct reactions have reached in the last few years a very good level of efficiency. Refinements in the measurement of fusion and direct reactions will continue with the nuclei currently available at radioactive beam facilities.

In the future however, further *exclusive* measurements of the direct reaction processes, such as those already carried out for the ${}^6\text{He} + {}^{209}\text{Bi}$ system [57, 58], are needed to help unravel the competition between breakup and transfer for neutron halo nuclei. One may eventually hope to have angular distribution measurements for a more detailed comparison with calculations. To reach this goal the implementation of different simultaneous signatures — charged particles, prompt γ -ray emission and neutron detection — is required. This calls for collaborations where expertise is brought together in some key experiments. The choice of the systems to measure will have to take into account the experimental constraints but also the theoretical ones as we have illustrated above.

Acknowledgements

The authors would like to thank Dr. A. Di Pietro, Prof. Yu. Penionzhkevich, Prof. J.J. Kolata, Prof. C. Signorini and Dr. M. Dasgupta for providing their data in tabular form; Prof. A. Vitturi and Dr. A. Navin for stimulating and instructive discussions. N.K. gratefully acknowledges the receipt of a Marie Curie Intra-European Fellowship from the European Commission, contract No. MEIF-CT-2005-010158. R.R. is a Postdoctoral Fellow of the Fund for Scientific Research-Flanders (Belgium) (F.W.O.-Vlaanderen).

References

- [1] R. J. Glauber, Phys. Rev. **100**, 242 (1955).
- [2] C. Y. Wong, Phys. Rev. Lett. **31**, 766 (1973).
- [3] G. R. Satchler, *Introduction to nuclear reactions*, 2nd ed. (MacMillan Education Ltd., London, 1990).
- [4] M. Beckerman, Phys. Rep. **129**, 145 (1985).
- [5] S. G. Steadman and M. J. Rhoades-Brown, Ann. Rev. Nucl. Part. Sci. **36**, 649 (1986).
- [6] I. Tanihata *et al.*, Phys. Rev. Lett. **55**, 2676 (1985).
- [7] I. Tanihata *et al.*, Phys. Lett. B **160**, 380 (1985).
- [8] J. S. Al-Khalili and J. A. Tostevin, Phys. Rev. Lett. **76**, 3903 (1996).
- [9] M. S. Hussein, M. P. Pato, L. F. Canto, and R. Donangelo, Phys. Rev. C **46**, 377 (1992).
- [10] C. H. Dasso and A. Vitturi, Phys. Rev. C **50**, R12 (1994).
- [11] A. O. Caldeira and A. J. Leggett, Phys. Rev. Lett. **46**, 211 (1981).
- [12] W. J. Swiatecki, Phys. Scr. **24**, 113 (1981).
- [13] J. Pampus *et al.*, Nucl. Phys. A **311**, 141 (1978).
- [14] T. Udagawa and T. Tamura, Phys. Rev. C **21**, 1271 (1980).
- [15] E. Takada *et al.*, Phys. Rev. C **23**, 772 (1981).
- [16] V. Tripathi *et al.*, Phys. Rev. C **72**, 017601 (2005).
- [17] K. Hagino, M. Dasgupta, and D. J. Hinde, Nucl. Phys. A **738**, 475 (2004).
- [18] R. Raabe *et al.*, Nature **431**, 823 (2004).
- [19] A. Di Pietro *et al.*, Phys. Rev. C **69**, 044613 (2004).
- [20] A. Navin *et al.*, Phys. Rev. C **70**, 044601 (2004).
- [21] M. Beckerman *et al.*, Phys. Rev. Lett. **45**, 1472 (1980).
- [22] R. G. Stokstad *et al.*, Z. Phys. A **295**, 269 (1980).

- [23] K. Rusek *et al.*, Phys. Rev. C **70**, 014603 (2004).
- [24] J. J. Kolata *et al.*, Phys. Rev. Lett. **81**, 4580 (1998).
- [25] M. Dasgupta *et al.*, Phys. Rev. Lett. **82**, 1395 (1999).
- [26] I. Padron *et al.*, Phys. Rev. C **66**, 044608 (2002).
- [27] A. M. Moro and F. M. Nunes, Nucl. Phys. A **767**, 138 (2006).
- [28] J. O. Newton *et al.*, Phys. Rev. C **70**, 024605 (2004).
- [29] M. Beckerman *et al.*, Phys. Rev. C **25**, 837 (1982).
- [30] P. R. S. Gomes, J. Lubian, I. Padron, and R. M. Anjos, Phys. Rev. C **71**, 017601 (2005).
- [31] H. Geissel, G. Munzenberg, and K. Riisager, Ann. Rev. Nucl. Part. Sci. **45**, 163 (1995).
- [32] C. Signorini *et al.*, Eur. Phys. J. A **2**, 227 (1998).
- [33] G. Ryckewaert *et al.*, Nucl. Phys. A **701**, 323c (2002).
- [34] A. Joubert *et al.*, in *Particle Accelerator Conference* (IEEE Proc., Washington, DC, USA, 1993), Vol. 2, pp. 1789–1791.
- [35] G. G. Gulbekian and Y. T. Oganessian, in *Nuclear shells - 50 Years, Proceedings of the 49th Meeting on Nuclear Spectroscopy and Nuclear Structure* (World Scientific, Singapore, 1999).
- [36] J. J. Kolata *et al.*, Nucl. Instrum. Methods Phys. Res. B **40-41**, 503 (1989).
- [37] M. Y. Lee *et al.*, Nucl. Instrum. Methods Phys. Res. A **422**, 536 (1999).
- [38] F. D. Becchetti *et al.*, Nucl. Instrum. Methods Phys. Res. A **505**, 377 (2003).
- [39] R. Lichtenthaler *et al.*, Braz. J. Phys. **33**, 294 (2003).
- [40] P. R. S. Gomes *et al.*, Nucl. Instrum. Methods Phys. Res. A **280**, 395 (1989).
- [41] P. Figuera *et al.*, in *Rapport d'activité CYCLONE 2004* (Institut de Physique Nucléaire et Centre de Recherches du Cyclotron, Louvain-la-Neuve, Belgium, 2005), p. 13.
- [42] A. Musumarra *et al.*, Nucl. Instrum. Methods Phys. Res. A **428**, 414 (1998).
- [43] R. Vandenbosch and J. R. Huizenga, *Nuclear Fission* (Academic Press, New York, 1973).
- [44] M. Dasgupta *et al.*, Phys. Rev. C **70**, 024606 (2004).
- [45] A. H. Wuosmaa *et al.*, Phys. Lett. B **172**, 297 (1986).
- [46] M. Dasgupta *et al.*, Phys. Rev. Lett. **66**, 1414 (1991).
- [47] L. F. Canto, P. R. S. Gomes, R. Donangelo, and M. S. Hussein, Phys. Rep. **424**, 1 (2006).
- [48] A. Di Pietro *et al.*, Europhys. Lett. **64**, 309 (2003).
- [49] A. Di Pietro *et al.*, Phys. Atom. Nucl. **69**, 1366 (2006).

- [50] Y. E. Penionzhkevich, V. I. Zagrebaev, S. M. Lukyanov, and R. Kalpakchieva, Phys. Rev. Lett. **96**, 162701 (2006).
- [51] V. I. Zagrebaev, Phys. Rev. C **67**, 061601 (2003).
- [52] V. I. Zagrebaev, Prog. Theor. Phys. Suppl. **154**, 122 (2004).
- [53] J. J. Kolata *et al.*, Phys. Rev. C **57**, R6 (1998).
- [54] P. A. DeYoung *et al.*, Phys. Rev. C **58**, 3442 (1998).
- [55] E. F. Aguilera *et al.*, Phys. Rev. C **63**, 061603(R) (2001).
- [56] E. F. Aguilera *et al.*, Phys. Rev. Lett. **84**, 5058 (2000).
- [57] J. P. Bychowski *et al.*, Phys. Lett. B **596**, 26 (2004).
- [58] P. A. DeYoung *et al.*, Phys. Rev. C **71**, 051601 (2005).
- [59] P. H. Stelson *et al.*, Phys. Rev. C **41**, 1584 (1990).
- [60] Y. E. Penionzhkevich, Nucl. Phys. A **588**, 259c (1995).
- [61] A. S. Fomichev *et al.*, Z. Phys. A **351**, 129 (1995).
- [62] Y. E. Penionzhkevich *et al.*, Eur. Phys. J. A **13**, 123 (2002).
- [63] M. Trotta *et al.*, Phys. Rev. Lett. **84**, 2342 (2000).
- [64] H. Freiesleben, G. T. Rizzo, and J. R. Huizenga, Phys. Rev. C **12**, 42 (1975).
- [65] R. Raabe *et al.*, Phys. Rev. C **74**, 044606 (2006).
- [66] A. Yoshida *et al.*, Phys. Lett. B **389**, 457 (1996).
- [67] C. Signorini *et al.*, Nucl. Phys. A **735**, 329 (2004).
- [68] C. Signorini *et al.*, Eur. Phys. J. A **5**, 7 (1999).
- [69] C. Signorini *et al.*, Eur. Phys. J. A **10**, 249 (2001).
- [70] M. Mazzocco *et al.*, Eur. Phys. J. A **28**, 295 (2006).
- [71] K. Rusek, N. Keeley, K. W. Kemper, and R. Raabe, Phys. Rev. C **67**, 041604(R) (2003).
- [72] N. Keeley *et al.*, Phys. Rev. C **68**, 054601 (2003).
- [73] K. Rusek *et al.*, Phys. Rev. C **72**, 037603 (2005).
- [74] T. Matsumoto *et al.*, Nucl. Phys. A **738**, 471 (2004).
- [75] A. M. Moro *et al.*, Phys. Rev. C **68**, 034614 (2003).
- [76] M. Takashina, S. Takagi, Y. Sakuragi, and Y. Iseri, Phys. Rev. C **67**, 037601 (2003).
- [77] T. Matsumoto *et al.*, Phys. Rev. C **73**, 051602 (2006).
- [78] I. J. Thompson, M. A. Nagarajan, J. S. Lilley, and B. R. Fulton, Phys. Lett. B **157**, 250 (1985).

- [79] S. C. Pieper, M. J. Rhoades-Brown, and S. Landowne, Phys. Lett. B **162**, 43 (1985).
- [80] N. Keeley, J. S. Lilley, and J. A. Christley, Nucl. Phys. A **603**, 97 (1996).
- [81] N. Keeley *et al.*, Nucl. Phys. A **628**, 1 (1998).
- [82] D. Pereira *et al.*, Phys. Rev. C **73**, 014601 (2006).
- [83] G. R. Satchler, *Direct nuclear reactions* (Oxford University Press, New York, 1983).
- [84] L. C. Vaz, J. M. Alexander, and G. R. Satchler, Phys. Rep. **69**, 373 (1981).
- [85] M. Beckerman, Rep. Prog. Phys. **51**, 1047 (1988).
- [86] M. Dasgupta, D. J. Hinde, N. Rowley, and A. M. Stefanini, Ann. Rev. Nucl. Part. Sci. **48**, 401 (1998).
- [87] G. H. Rawitscher, Phys. Rev. C **9**, 2210 (1974).
- [88] P. Chau Huu-Tai, Nucl. Phys. A **773**, 56 (2006).
- [89] Y. Sakuragi, M. Yahiro, and M. Kamimura, Prog. Theor. Phys. **68**, 322 (1982).
- [90] Y. Sakuragi, M. Yahiro, and M. Kamimura, Prog. Theor. Phys. Suppl. **89**, 136 (1986).
- [91] T. Yamagata *et al.*, Phys. Rev. C **39**, 873 (1989).
- [92] Y. Sakuragi, M. Yahiro, and M. Kamimura, Prog. Theor. Phys. **70**, 1047 (1983).
- [93] Y. Sakuragi, Phys. Rev. C **35**, 2161 (1987).
- [94] N. Austern *et al.*, Phys. Rep. **154**, 125 (1987).
- [95] T. Matsumoto *et al.*, Phys. Rev. C **70**, 061601 (2004).
- [96] N. C. Summers, F. M. Nunes, and I. J. Thompson, Phys. Rev. C **73**, 031603 (2006).
- [97] N. C. Summers, F. M. Nunes, and I. J. Thompson, Phys. Rev. C **74**, 014606 (2006).
- [98] A. Diaz-Torres, I. J. Thompson, and C. Beck, Phys. Rev. C **68**, 044607 (2003).
- [99] N. Keeley, K. W. Kemper, and K. Rusek, Phys. Rev. C **64**, 014601 (2002).
- [100] V. I. Kukulín and R. S. Mackintosh, J. Phys. G **30**, R1 (2004).
- [101] I. J. Thompson, M. A. Nagarajan, J. S. Lilley, and M. J. Smithson, Nucl. Phys. A **505**, 84 (1989).
- [102] C. H. Dasso, S. Landowne, and A. Winther, Nucl. Phys. A **405**, 381 (1983).
- [103] M. J. Rhoades-Brown and P. Braun-Munzinger, Phys. Lett. B **136**, 19 (1984).
- [104] M. Ito, K. Yabana, T. Nakatsukasa, and M. Ueda, Phys. Lett. B **637**, 53 (2006).
- [105] J. Raynal, Phys. Rev. C **23**, 2571 (1981).
- [106] M. J. Rhoades-Brown, M. H. Macfarlane, and S. C. Pieper, Phys. Rev. C **21**, 2417 (1980).
- [107] I. J. Thompson, Comput. Phys. Rep. **7**, 167 (1988).

- [108] K. Hagino, N. Rowley, and A. T. Kruppa, *Comput. Phys. Commun.* **123**, 143 (1999).
- [109] N. Keeley, N. Alamanos, K. Rusek, and K. W. Kemper, *Phys. Rev. C* **71**, 014611 (2005).
- [110] G. M. Hudson and R. H. Davis, *Phys. Rev. C* **9**, 1521 (1974).
- [111] A. Warwick, R. Chapman, J. L. Durell, and J. N. Mo, *Phys. Lett. B* **87**, 335 (1979).
- [112] Å. Bredback *et al.*, *Nucl. Phys. A* **574**, 397 (1994).
- [113] S. B. Sakuta, D. N. Stepanov, and Y. Tseipek, *Sov. J. Nucl. Phys.* **49**, 953 (1989).
- [114] M. M. Alam and F. B. Malik, *Phys. Lett. B* **237**, 14 (1990).
- [115] D. J. Pullen, J. R. Rook, and R. Middleton, *Nucl. Phys.* **51**, 88 (1964).
- [116] R. S. Mackintosh, *Nucl. Phys. A* **230**, 195 (1974).
- [117] A. A. Ioannides and R. S. Mackintosh, *Nucl. Phys. A* **467**, 482 (1987).
- [118] R. S. Mackintosh, S. G. Cooper, and A. A. Ioannides, *Nucl. Phys. A* **472**, 85 (1987).
- [119] G. R. Satchler and W. G. Love, *Phys. Rep.* **55**, 183 (1979).
- [120] G. R. Satchler and W. G. Love, *Phys. Lett. B* **76**, 23 (1978).
- [121] M. F. Steeden *et al.*, *J. Phys. G* **6**, 501 (1980).
- [122] G. R. Satchler, *Phys. Lett. B* **83**, 284 (1979).
- [123] R. S. Mackintosh and A. M. Kobos, *Phys. Lett. B* **116**, 95 (1982).
- [124] M. A. Nagarajan, I. J. Thompson, and R. C. Johnson, *Nucl. Phys. A* **385**, 525 (1982).
- [125] Y. Hirabayashi, S. Okabe, and Y. Sakuragi, *Phys. Lett. B* **221**, 227 (1989).
- [126] N. Alamanos *et al.*, *Phys. Rev. C* **65**, 054606 (2002).
- [127] C. Signorini *et al.*, *Phys. Rev. C* **67**, 044607 (2003).
- [128] A. Pakou *et al.*, *Phys. Lett. B* **633**, 691 (2006).
- [129] N. Keeley *et al.*, *Nucl. Phys. A* **571**, 326 (1994).
- [130] N. Keeley and K. Rusek, *Phys. Lett. B* **375**, 9 (1996).
- [131] I. Tanihata *et al.*, *Phys. Lett. B* **289**, 261 (1992).
- [132] J. Cook and K. W. Kemper, *Arabian Journal for Science and Engineering* **8**, 331 (1983).
- [133] A. I. Steshenko, *Phys. Atomic Nuclei* **60**, 520 (1997).
- [134] T. Neff and H. Feldmeier, *Nucl. Phys. A* **738**, 357 (2004).
- [135] H. Euteneuer, J. Friedrich, and N. Voegler, *Nucl. Phys. A* **298**, 452 (1978).
- [136] R. M. Lombard, G. D. Alkhazov, and O. A. Domchenkov, *Nucl. Phys. A* **360**, 233 (1981).

- [137] J. Cook, *Comput. Phys. Commun.* **25**, 125 (1982).
- [138] D. G. Kovar, N. Stein, and C. K. Bockelman, *Nucl. Phys. A* **231**, 266 (1974).
- [139] O. F. Nemets *et al.*, *Nucleon clusters in atomic nuclei and many-nucleon transfer reactions (in Russian)* (Ukrainian Academy of Sciences, Institute for Nuclear Research, Kiev, 1988).
- [140] F. Skaza *et al.*, *Phys. Lett. B* **619**, 82 (2005).
- [141] S. Cohen and D. Kurath, *Nucl. Phys.* **101**, 1 (1967).
- [142] E. Wesolowski *et al.*, *J. Phys. G* **17**, 955 (1991).
- [143] R. Ost *et al.*, *Z. Phys. A* **266**, 369 (1974).
- [144] J. Cook, *NPA* **388**, 153 (1982).
- [145] Y. W. Wu *et al.*, *Phys. Rev. C* **68**, 044605 (2003).
- [146] C. Signorini *et al.*, *Nuovo Cim.* **111 A**, 917 (1998).
- [147] A. Bhagwat, Y. K. Gambhir, and S.H.Patil, *Eur. Phys. J. A* **8**, 511 (2000).
- [148] H. Sagawa, *Phys. Lett. B* **7**, 286 (1992).
- [149] J. S. McCarthy, I. Sick, and R. R. Whitney, *Phys. Rev. C* **15**, 1396 (1977).
- [150] W. Kegel, Master's thesis, University of Amsterdam, 1977, cited in: H. De Vries, C. W. De Jager, and C. De Vries, *At. Data Nucl. Data Tables* 36 (1987) 495.
- [151] T. Cooper *et al.*, *Phys. Rev. C* **13**, 1083 (1976).
- [152] H. J. Gils and H. Rebel, *Phys. Rev. C* **13**, 2159 (1976).
- [153] D. T. Khoa, G. R. Satchler, and W. von Oertzen, *Phys. Rev. C* **56**, 954 (1997).
- [154] J. S. Al-Khalili, J. A. Tostevin, and I. J. Thompson, *Phys. Rev. C* **54**, 1843 (1996).
- [155] F. Pühlhofer, *Nucl. Phys. A* **280**, 267 (1977).
- [156] V. E. Viola and T. Sikkeland, *Phys. Rev.* **128**, 767 (1962).
- [157] N. I. Zaika *et al.*, *Sov. J. Nucl. Phys.* **31**, 22 (1980).
- [158] V. N. Levkovskij, *Activation Cross Sections by Protons and Alphas*, Moscow (1991), data file EXFOR-A0510.
- [159] F. H. Ruddy and B. D. Pate, *Nucl. Phys. A* **127**, 305 (1969).
- [160] N. T. Porile, *Phys. Rev.* **115**, 939 (1959).
- [161] A. R. Barnett and J. S. Lilley, *Phys. Rev. C* **9**, 2010 (1974).
- [162] W. J. Ramler, J. Wing, D. J. Henderson, and J. R. Huizenga, *Phys. Rev.* **114**, 154 (1959).
- [163] C. Signorini, *Eur. Phys. J. A* **13**, 129 (2002).
- [164] K. Hagino, A. Vitturi, C. H. Dasso, and S. M. Lenzi, *Phys. Rev. C* **61**, 037602 (2000).

- [165] A. Diaz-Torres and I. J. Thompson, Phys. Rev. C **65**, 024606 (2002).
- [166] N. Keeley, K. W. Kemper, and K. Rusek, Phys. Rev. C **66**, 044605 (2002).
- [167] N. Takigawa and H. Sagawa, Phys. Lett. B **265**, 23 (1991).
- [168] E. Vulgaris, L. Grodzins, S. G. Steadman, and R. Ledoux, Phys. Rev. C **33**, 2017 (1986).